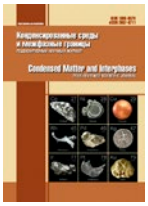

ISSN 1606-867X (Print)
ISSN 2687-0711 (Online)
Condensed Matter and Interphases
Kondensirovannye Sredy i Mezhfaznye Granitsy
https://journals.vsu.ru/kcmf/

Review

Review article
https://doi.org/10.17308/kcmf.2024.26/12397

Phase transformations in systems formed by titanium, silicon, aluminum, and zirconium oxides: Phase diagrams prediction and modeling. Review

V. I. Lutsyk, A. E. Zelenaya✉, V. P. Vorob'eva

Institute of Physical Materials Science, Siberian Branch of the Russian Academy of Sciences,
6 Sakhyanova st., Ulan-Ude 670047, Russian Federation

Abstract

This paper provides a review of variants of phase diagrams of binary and ternary systems constituting the TiO_2-Al_2O_3-SiO_2-ZrO_2 four-component system.

The study involved building spatial (three-dimensional (3D)) computer models of the isobaric phase diagrams for four ternary oxide systems (and their variants, in case of contradicting initial data obtained by different researchers) constituting this quaternary system. The geometric structure of its phase diagram was also predicted. For this purpose, phase diagram models were constructed as geometric objects in three-dimensional (3D) or four-dimensional (4D) space in the "concentration-temperature" coordinates by assembling (hyper)surfaces (unruled and ruled) and/or phase regions.

As a result:

– For the TiO_2-Al_2O_3-SiO_2 system, it was considered possible variants of the structure of liquidus surfaces. These variations were due to availability of different theories describing the formation of compounds in the TiO_2-Al_2O_3 binary system (Al_2TiO_5 can melt congruently or incongruently and either possesses or does not possess the property of polymorphism).

– For the TiO_2-Al_2O_3-ZrO_2 and TiO_2-SiO_2-ZrO_2 systems, 3D-models of phase diagrams were developed at temperatures above 1,280 and 1,400 °C, respectively. The temperature limits were due to the lack of definitive description of the structure of subsolidus regions in the TiO_2-ZrO_2 binary boundaring system.

– Since the main contradictions in the ZrO_2-SiO_2-Al_2O_3 system are associated with the type of phase reaction related to zircon formation (peritectic or peritectoid), the 3D model of the phase diagram was built according to the second variant, which involved the formation of the internal field of liquidus corresponding to the primary crystallization of $ZrSiO_4$.

The structure of the phase diagrams in the subsolidus was deduced for all four systems. It was also shown that in these systems at decreasing of temperature triangulation had a place twice.

For the TiO_2-Al_2O_3-SiO_2-ZrO_2 quaternary system, a scheme of phase reactions with the participation of the melt was deduced. This scheme includes six five-phase invariant reactions: two peritectic, two eutectic, and two quasi-peritectic reactions.

Keywords: Phase diagrams, Computer modeling, Four-dimensional visualization, Titanium, aluminum, Silicon, and Zirconium oxides

Funding: This work was performed under the program of fundamental research of the Institute of Physical Materials Science of the Siberian Branch of the Russian Academy of Sciences, project No. 0270-2024-0013.

For citation: Lutsyk V. I., Zelenaya A. E., Vorob'eva V. P. Phase transformations in systems formed by titanium, silicon, aluminum, and zirconium oxides: Phase diagrams prediction and modeling. Review. *Condensed Matter and Interphases*. 2024;25(3): 666–686. https://doi.org/10.17308/kcmf.2024.26/12397

Для цитирования: Луцык В. И., Зеленая А. Э., Воробьева В. П. Фазовые превращения в системах, образованных оксидами титана, кремния, алюминия, циркония: прогноз и моделирование фазовых диаграмм. Обзор. *Конденсированные среды и межфазные границы*. 2024;25(3): 666–686. https://doi.org/10.17308/kcmf.2024.26/12397

✉ Anna E. Zelenaya, e-mail: zel_ann@mail.ru

1. Introduction

Innovative ceramics based on ZTA, a combination of zirconium, titanium, and aluminum oxides, have a wide range of practical applications. Therefore, there is a need to provide a precise and experiment-consistent description of isobaric phase diagrams for both the ternary systems formed by ZTA and SiO_2 and the TiO_2-Al_2O_3-SiO_2-ZrO_2 quaternary system. Phase diagrams of its binary systems are very contradictory, which is associated with disagreements on the properties of the compounds formed within these systems (the presence or absence of polymorphism, the nature of the formation, and the type of melting).

2. Literature review

It is known that silicon and zirconium oxides, which together with titanium and aluminum oxides form the TiO_2-Al_2O_3-SiO_2-ZrO_2 system, have several polymorphic modifications. Zirconium (IV) oxide has three modifications: cubic (*c*-ZrO_2), tetragonal (*t*-ZrO_2), and monoclinic (*m*-ZrO_2) [1–3]. Silicon (IV) oxide has four modifications: cristobalite (*cr*-SiO_2), tridymite (*tr*-SiO_2), high-temperature quartz (HQ-SiO_2), and low-temperature quartz (LQ-SiO_2) [1].

2.1. Binary systems in the TiO_2-Al_2O_3-SiO_2-ZrO_2 four-component system

The Al_2O_3-ZrO_2 system has the simplest geometric structure of the six considered binary systems constituting TiO_2-Al_2O_3-SiO_2-ZrO_2 (Fig. 1a). Experimental [2-5] and thermodynamically calculated [6, 7] data indicate that there is an eutectic reaction between Al_2O_3 and the tetragonal form of zirconium oxide (*t*-ZrO_2), the *c*-ZrO_2 → *t*-ZrO_2 + L metatectic polymorphic transition, and the eutectoid transition from the tetragonal *t*-ZrO_2 to the monoclinic *m*-ZrO_2 [2].

In the TiO_2-SiO_2 eutectic system (Fig. 1b), in addition to liquid immiscibility, there are three polymorphic transitions from cristobalite (*cr*-SiO_2) to tridymite (*tr*-SiO_2) and further to high and low-temperature quartzes (HQ-SiO_2 and LQ-SiO). This system has been studied in many papers [8–21]. All researchers agree that the system is characterized by liquid immiscibility and the eutectic reaction. Their opinions only differ with regard to the values of the coordinates of the eutectic reaction and the dimensions of the liquid immiscibility region, both in terms of its composition and temperature.

The SiO_2-ZrO_2 system (Fig. 1c) has an immiscibility region of two liquids and the $ZrSiO_4$ compound (zircon) [22–26]. The main differences in publications devoted to this system relate to the type of phase reaction by which this compound is formed: peritectic [22] or peritectoid. More recent studies confirm the peritectoid nature of the reaction [25]: *tr*-SiO_2 + *t*-ZrO_2 → $ZrSiO_4$ with the participation of tridymite and tetragonal form of zirconium oxide. In the subsolidus, zircon participates in low-temperature polymorphic transitions, in which polymorphic forms of SiO_2 and ZrO_2 also take part. The "liquidus" part of the phase diagram is characterized by a high-temperature metatectic transition from *c*-ZrO_2 to *t*-ZrO_2, liquid immiscibility, and the eutectic reaction. An overview of opinions on the structure of the ZrO_2-SiO_2 phase diagram is presented in [23–26].

The descriptions of the Al_2O_3-SiO_2 system provide different interpretations of the nature of mullite melting (mainly with the $Al_6Si_2O_{13}$ stoichiometry). In [27–48], it is defined either as congruent (then the mullite divides the system into two eutectic subsystems (Fig. 1d)), or as incongruent (then the mullite is formed by a peritectic reaction).

The TiO_2-ZrO_2 system has been extensively researched with the main differences in its description relating to the presence of zirconium titanate (Fig. 1e). The phase diagrams presented in [49] and [50] have a similar structure, but differ in the presence of the ordered and disordered phase of $ZrTiO_4$. Importantly, since there is no definitive description of phase transformations in this system, in this work we limited the modeling of the TiO_2-Al_2O_3-ZrO_2 and TiO_2-SiO_2-ZrO_2 ternary systems formed by them to the temperatures of 1,280 and 1,400 °C, respectively.

There are four main versions of phase transformations in the TiO_2-Al_2O_3 system. What they have in common is the recognition of the existence of aluminum titanate, however, they differ in the interpretations of the type of its melting (incongruent [51] (Fig. 1f) or congruent), the presence or absence of its second polymorphic modification, and/or the formation of one more compound $Al_6Ti_2O_{13}$ [52-63].

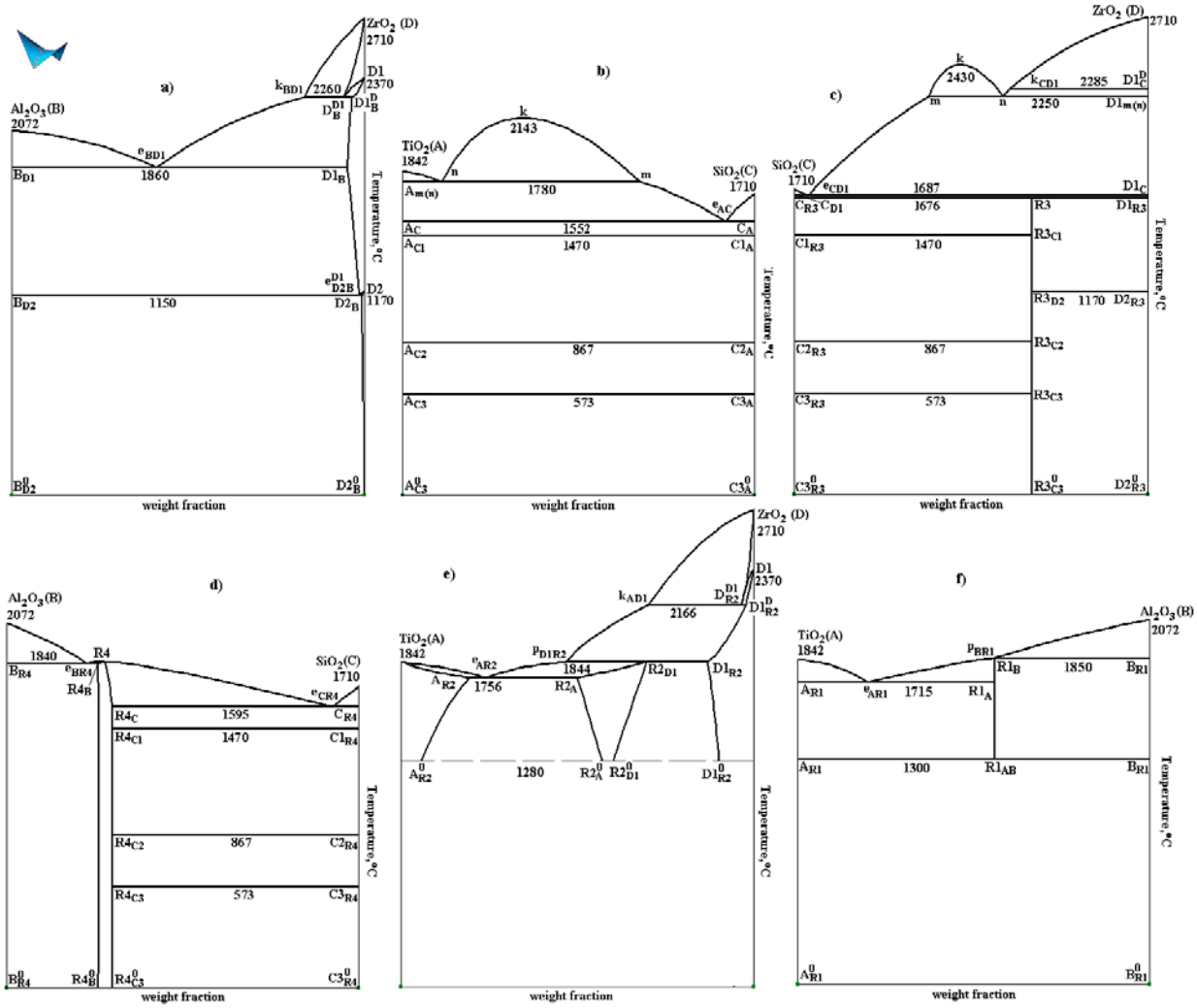

Fig. 1. Phase diagrams of binary systems: Al_2O_3-ZrO_2 (B-D) (a) [2, 7], TiO_2-SiO_2 (A-C) (b) [19], SiO_2-ZrO_2 (C-D) (c) [1], Al_2O_3-SiO_2 (B-C) (d) [30, 35], TiO_2-ZrO_2 (A-D) (e) [49], TiO_2-Al_2O_3 (A-B) (f) [51] with the formation of: titanates of aluminum Al_2TiO_5 (R1) and zirconium $ZrTiO_4$ (R2), zircon $ZrSiO_4$ (R3), mullite $Al_6Si_2O_{13}$ (R4) (C – cristobalite cr-SiO_2, C1 – tridymite *tr*-SiO_2, C2 – high-temperature HQ-SiO_2 and S3 – low-temperature LQ-SiO_2 quartz; D – cubic *c*-ZrO_2 , D1 – tetragonal *t*-ZrO_2, D2 - monoclinic *m*-ZrO_2 polymorphic modifications of ZrO_2)

2.2. Ternary systems in the TiO_2-Al_2O_3-SiO_2-ZrO_2 four-component system

The authors of the work [64] (cited from [65]) studied the phase diagram of the TiO_2-Al_2O_3-SiO_2 ternary system, rich in alumina, and established the presence of two invariant reactions, eutectic and quasi-peritectic (Fig. 2a):

E_1: $L \rightarrow TiO_2 + SiO_2 + Al_2TiO_5$ and
Q_2: $L + Al_6Si_2O_{13} \rightarrow SiO_2 + Al_2TiO_5$.

Later, a third invariant reaction was recorded, corresponding to another quasi-peritectic transformation [66]:

Q_1: $L + Al_2O_3 \rightarrow Al_6Si_2O_{13} + Al_2TiO_5$.

Studies [67] in the subsolidus region showed the presence of two phase regions: $TiO_2 + SiO_2 + Al_6Si_2O_{13}$ and $TiO_2 + Al_2TiO_5 + Al_6Si_2O_{13}$.

The authors of [68] experimentally recorded the same invariant reactions but with different melt compositions. They also established the presence of a quasi-peritectoid reaction in the solid-phase region: $SiO_2 + Al_2TiO_5 \rightarrow TiO_2 + Al_6Si_2O_{13}$.

Since there are four main variants of the structure of the phase diagram of the TiO_2-Al_2O_3 binary system, it is also possible to obtain four variants of the structure of the ternary systems constituted by this binary system together with silicon or zirconium oxides.

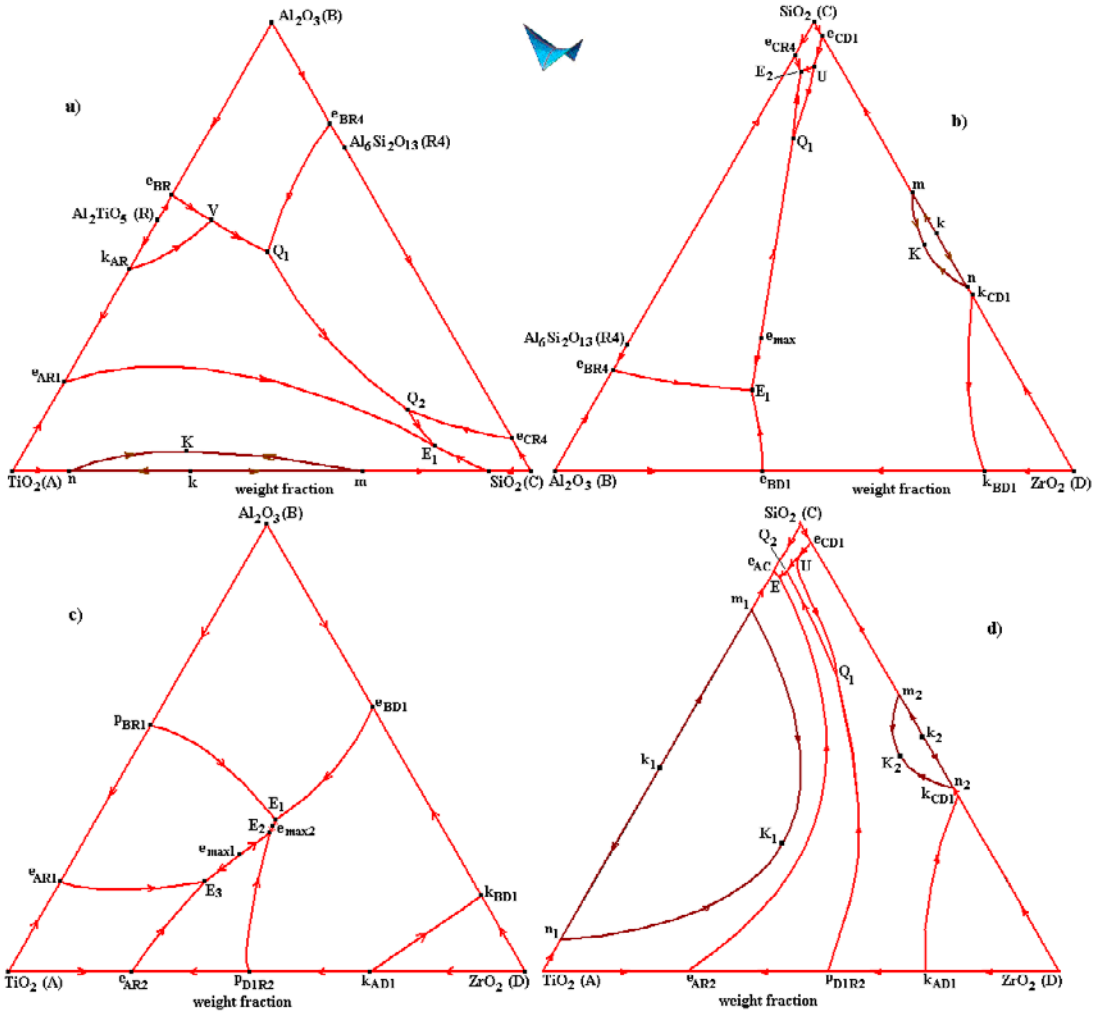

Fig. 2. Liquidus surfaces projections of the TiO_2-Al_2O_3-SiO_2 (A-B-C) (a), Al_2O_3-SiO_2-ZrO_2 (B-C-D) (b), TiO_2-Al_2O_3-ZrO_2 (A-B-D) (c), TiO_2-SiO_2-ZrO_2 (A-C-D) (d) systems with compounds Al_2TiO_5 (R1), $ZrTiO_4$ (R1), $ZrSiO_4$ (R3), $Al_6Si_2O_{13}$ (R4)

The liquidus of the TiO_2-Al_2O_3-SiO_2 ternary system consists of a region of liquid immiscibility and five surfaces of onset primary crystallization: three initial oxides and two binary compounds with aluminum titanate melting either incongruently or congruently. If we accept the version about the existence of two polymorphic modifications of aluminum titanate, according to which the low-temperature modification of aluminum titanate on the phase diagram of the TiO_2-Al_2O_3 binary system has the corresponding liquidus line (interestingly, it is only present in one subsystem with TiO_2, while in the other subsystem it can only be found in the subsolidus), then two fields of primary crystallization of aluminum titanate for both its polymorphic modifications appear in the ternary system (Fig. 2a). However, there is no information about liquidus surfaces corresponding to the onset crystallization of a low-temperature modification in any of the studies devoted to this ternary system. Data are only available for a high-temperature modification [17, 21, 64–68].

According to another version, in addition to the congruently melting aluminum titanate Al_2TiO_5, an incongruently melting compound $Al_6Ti_2O_{13}$ is formed. This means that a sixth field is present in the system corresponding to the primary crystallization of the compound.

To take into account the polymorphism of aluminum titanate (its two modifications), the listed Q_1, Q_2, and E_1 reactions must be preceded by an invariant four-phase polymorphic transition between the high-temperature and

low-temperature modifications of Al_2TiO_5 in the presence of Al_2O_3 and the melt in the temperature range of T_{eBR}-T_{Q1}. This transition corresponds to point V on the $e_{BR}Q_1$ line, where the liquidus field of the high-temperature modification of aluminum titanate closes (Fig. 2a). As a result, the surface of its liquidus consists of two fragments: $k_{AR}Re_{BR}V$ (primary crystallization of the high-temperature modification of Al_2TiO_5) and $e_{AR1}k_{AR}VQ_1Q_2E_1$ (separation of primary crystals of its low-temperature modification).

Thus, a large amount of contradictory data significantly complicates the task of constructing a quality model of the phase diagram. The lack of definitive experimental data about the structure of the TiO_2-Al_2O_3 binary system makes it difficult to obtain a single, unified, thermodynamically justified model of the phase diagram. A more effective solution in this case is building a geometric spatial model of the phase diagram, which will be discussed below.

Papers [69-71] present the results of studies, according to which, the liquidus of the Al_2O_3-SiO_2-ZrO_2 ternary system is characterized by six surfaces corresponding to the initial components (including two polymorphic forms of zirconium oxide), mullite, and zircon, and by quasi-peritectic and two eutectic reactions (Fig. 2b):

Q_1: L + *t*-ZrO_2 → $Al_6Si_2O_{13}$ + $ZrSiO_4$,
E_1: L → Al_2O_3 + *t*-ZrO_2 + $Al_6Si_2O_{13}$, E_2: L → → SiO_2 + $Al_6Si_2O_{13}$ + $ZrSiO_4$.

The main contradictions in this ternary system are associated with the structure of the liquidus and, in particular, the surface corresponding to the onset primary crystallization of the $ZrSiO_4$ zircon. The works [72-75] indicate the formation of five primary crystallization surfaces, including an internal field corresponding to $ZrSiO_4$, and four invariant reactions. Earlier, following the logic of the scheme of phase transformations, two phase reaction schemes were deduced corresponding to two variants of zircon formation [76]. The formation of zircon by the peritectoid reaction (Fig. 1c) results in the formation of the internal liquidus field of $ZrSiO_4$ and another invariant peritectic reaction (Fig. 2b):

L + *t*-ZrO_2 + SiO_2 → $ZrSiO_4$.

The description of the liquidus surfaces of the TiO_2-Al_2O_3-ZrO_2 system are contradictory. The structure of the diagram of TiO_2-ZrO_2 in the subsolidus can be interpreted in many ways. What is more, the discrepancies in the interpretation of the data related to the TiO_2-Al_2O_3 binary system also complicate the experimental study of the ternary system constituded by this binary system and aluminum oxide. According to [77], there are three eutectic transformations in this ternary system (Fig. 2c). Work [78, p. 107] presents the projection of the liquidus surfaces with three invariant points marked: two eutectic and one quasi-peritectic. The univariant liquidus line connecting the eutectic and quasi-peritectic points contains the maximum point located on the quasi-binary section of ZrO_2-Al_2TiO_5. Importantly, the point characterized as quasi-peritectic is located inside the ZrO_2-Al_2TiO_5-$ZrTiO_4$ simplex. However, such position of the point means that the phase reaction can only be eutectic in nature. Otherwise, in order to preserve the quasi-peritectic nature of the reaction corresponding to this point, it must be shifted to the TiO_2-Al_2TiO_5-$ZrTiO_4$ simplex. The projection of the liquidus surfaces obtained by thermodynamic calculations [79] has 4 invariant points.

Contradictory information about the TiO_2-ZrO_2 binary system [80, 81] (Fig. 2d) also significantly complicates the study of the phase diagram of the TiO_2-SiO_2-ZrO_2 system over the entire range of temperatures from the liquidus to subsolidus. The structure of the liquidus surfaces is shown in [82].

3. 3D modeling of isobaric phase diagrams of ternary systems

Currently, thermodynamic databases are widely used to describe phase equilibria in multicomponent systems, which make it possible to use the CALPHAD technology to produce precise calculations of phase diagrams [83, 84]. This approach allows calculating phase equilibria in multicomponent systems at high temperatures, for example, by using the NUCLEA database designed to simulate emergency situations at nuclear power plants [85, 86].

However, the limitations of using the results of the description of phase equilibria in the studied systems obtained by using the NUCLEA database include the representation of a significant number of phases as stoichiometric [86]. This also concerns mullite, the phase diagrams of which usually show the formation of a solid solution. Another limitation of the potential of the

NUCLEA database is a simplified understanding of the metatectic reactions associated with polymorphic transformations [87, Fig. 8].

Earlier [88], a thermodynamic database for the corresponding binary and ternary systems containing ZrO_2 was created to use the CALPHAD approach for calculations of phase diagrams. This allowed to avoid distortions in the image of metatectic reactions and to calculate the surface of the liquidus and fourteen polythermal sections of the Al_2O_3-SiO_2-ZrO_2 phase diagram.

One of the complications related to the construction of phase diagrams of multicomponent systems is the presence of polymorphic modifications of initial components and compounds formed in the system. This is especially true in cases of limited solubility of the polymorphic modifications of compounds within the studied system, which should also be taken into account.

3.1. Key provisions related to the construction of phase diagrams of ternary systems from the surfaces/phase regions

Good results related to the modeling of isobaric phase diagrams have been shown by an approach that allows assembling phase diagrams from the surfaces and/or phase regions. These diagrams can be further used to develop their spatial computer models. According to [89–94], such approach allows:

– Considering in detail the features of the physicochemical characteristics of the studied system, for example, negligibly small mutual solubility of the phases and the peculiarities of the solidus structure in a three-component system with immiscibility present in the melt.

– Freely operating with phase diagrams, including visualization of various isothermal and polythermal sections.

– Taking into account all surfaces and phase regions of the phase diagram.

– Correctly interpreting various experimental and calculated data on phase equilibria displayed on the isothermal and polythermal sections.

To build computer models of phase diagrams, the PD Designer and Neditor programs are used to assemble phase diagrams from the surfaces and/or phase regions [92, 95–98].

The initial data used to build a computer model include both experimental and matching thermodynamic data on binary boundaring systems and the surfaces of primary crystallization with due account of the nature of the melting (decomposition) of the binary and ternary compounds present in the system.

The assembly of the phase diagram from the surfaces and phase regions for spatial (3D) computer model involves several steps: 1) scheme of mono- and invariant states presented in a tabulated (Table 1) and graphical (Fig. 3) forms; 2) prototype of the phase diagram; 3) computer 3D model of the phase diagram of the real system.

The scheme of mono- and invariant states presented in a tabulated form is similar to Scheil's scheme of phase reactions; however, it includes attributed trajectories of changes in phase compositions during three-phase transformations. This allowes to directly obtain from the scheme detailed information about the geometrical structure of the phase diagram, i.e. about the number and type of all surfaces and phase regions. Such a table is very helpful since it is very convenient to track (or predict) the sequence of phase transformations not only with the participation of the melt, but also in the subsolidus.

Further, the two-dimensional (tabulated) scheme is transformed into the spacial scheme with due account of the location of points by temperature. In other words, the tabulated form is converted into geometric in the "concentration-temperature" coordinates. First, all the planes corresponding to the invariant transformations in the ternary system are constructed. Then, segments the ends of which are indicated in the scheme and which correspond to the changes in the compositions of the phases (participating in three-phase transformations) are brought to these planes [90]. Thus, the template of the phase diagram is formed.

The template is then completed with the surfaces imitating the surfaces of liquidus, solidus, solvus, and transus and phase regions are formed. The resulting prototype of a computer 3D model gives a deep understanding of the structure of the phase diagram.

The ruled surfaces are formed by the generating segment and two directing curves and comprised the boundaries of the corresponding three-phase transformation. All other surfaces (liquidus, solidus, solvus, transus, etc) are unruled. It is obvious that kinematic method is used to generate the ruled surface. In many cases, this method also

Table 1. Scheme of uni- and invariant states of the Al_2O_3-SiO_2-ZrO_2 (B-C-D) system with compounds $ZrSiO_4$ (R3) и $Si_2Al_6O_{13}$ (R4), D>k>D1(k_{CD1})>k_{BD1}>m(n)>B>e_{BD1}>R4>e_{BR4}> >e_{max}>E_1>C>e_{CD1}>R3>U>Q_1>e_{CR4}> E_2>C1(e^C_{C1R3},e^C_{C1R4},E_4)>P>D2(e^{D1}_{D2R3}>E_3)>e^{D1}_{BD2}>Q_2> >C2(e^{C1}_{C2R3},e^{C1}_{C2R4},E_5)>C3(e^{C2}_{C3R3},e^{C2}_{C3R4},E_6)

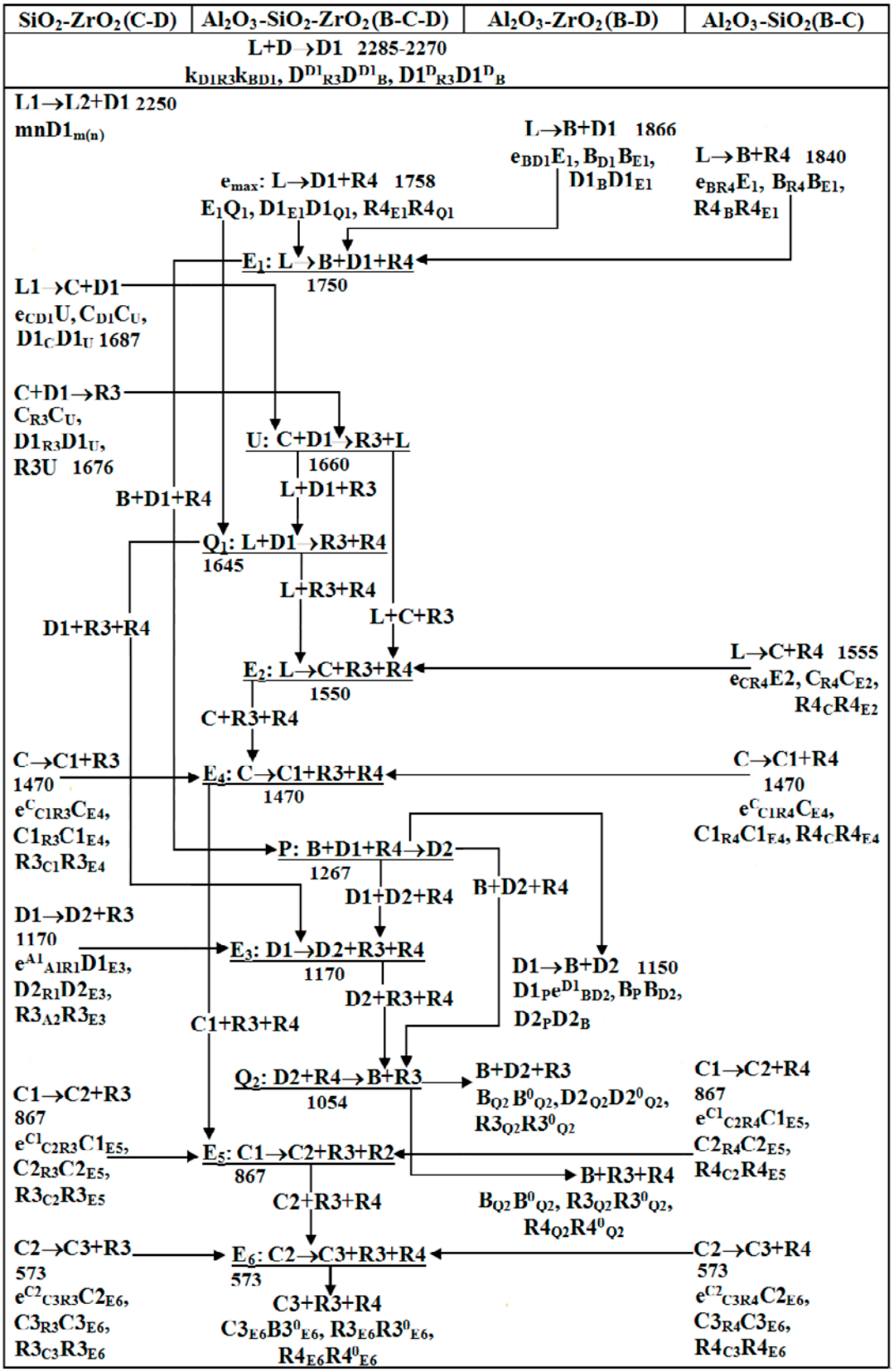

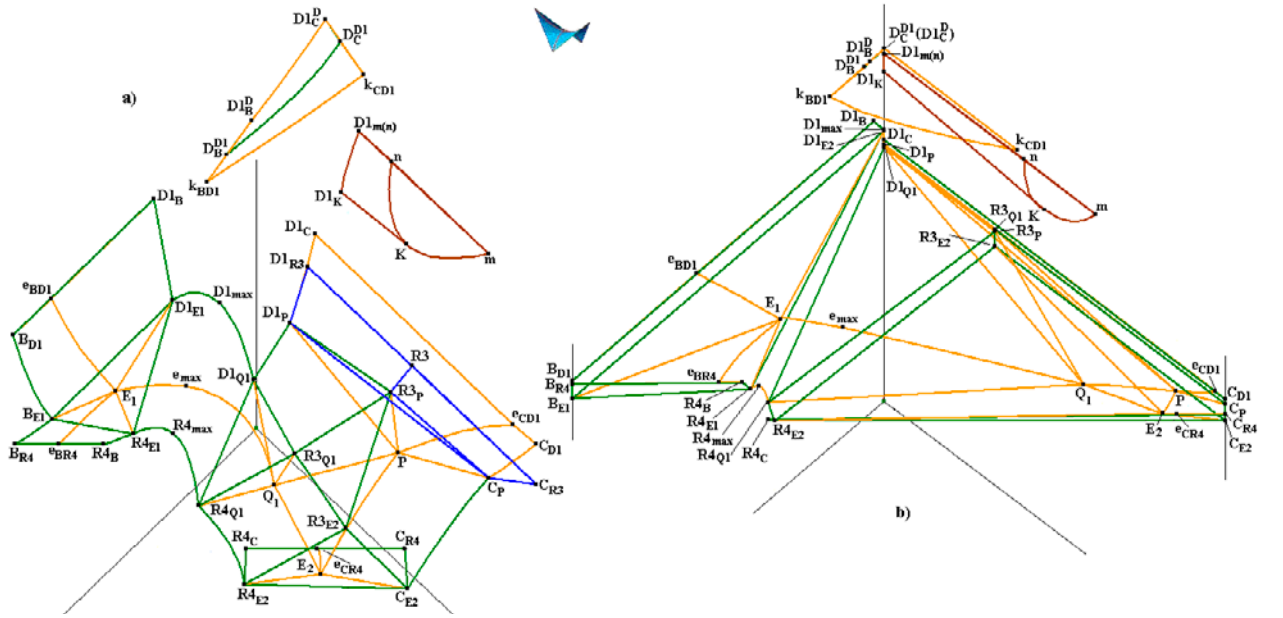

Fig. 3. Fragment of a 3D scheme of uni- and invariant states with a melt participation: a prototype (a), a real Al_2O_3-SiO_2-ZrO_2 (B-C-D) system with the formation of zircon Zr_3SiO_4 (R3) and mullite $Al_6Si_2O_{13}$ (R4) (b)

allows properly representing unruled surfaces as the movement of the generating element along the directing curves. Then, the surface is determined using directing and generating curves specified by Lagrange interpolation polynomials of *m* degree. This approach allows taking into account the presence of Van Rijn points, the curvature of the curves on the contour of the surfaces, the convexity of the surfaces, and the complex contour of the surfaces.

If the kinematic method cannot "cover" the entire surface (for example, when there is a fold, i.e. immiscibility region), it is divided into fragments. Then, the problem of proper representation of the surface is reduced to "merging" the surface from the fragments with mandatory control of equalizing derivatives at the points of their connection.

It should be noted that an important stage in phase diagram modeling is the construction of its prototype. A prototype is an ideal design of a phase diagram: i.e. a hypothetical phase diagram that completely reproduces the structure of the real phase diagram; it is its topological analogue comprising surfaces degenerated in a real system.

Moreover, the surfaces must be constructed in such a way as to give the best idea of both the surfaces themselves and the phase regions, for which these surfaces serve as the boundaries. To achieve this, the base points coordinates (concentrations and temperatures) are given so that the surfaces are not degenerated into the faces or verticals of the prism within which they are constructed.

To convert the prototype into a 3D model of the phase diagram of a real system, the real coordinates of all base points are first given and those surfaces that merge with the facets of the phase diagram (i.e. edges and faces of the prism) are "degenerated". The next stage deal with providing accurate and sound representation of the available experimental data (or information obtained from various sources, including thermodynamic calculations). To do this, the curvatures of lines and surfaces are specified and, as a result, a spatial computer model of a particular phase diagram is obtained. The process of obtaining a perfect model can be long; it may require additional clarifying experiments. However, it can be sure that the computer model of the phase diagram constructed in such a way has no methodological errors caused by an incorrect interpretation of the experiment that can occur when constructing phase diagrams using conventional methods [93, 94].

It is important to highlight that despite the fact that the limited solubility of some oxides and compounds is negligibly low, the 3D model makes it possible to take into account all surfaces and phase regions, and thus the phase diagram is protected

from errors. The obtained models can be used as the basis for further planning of experiments, while the approach to building spatial computer models of phase diagrams of ternary and more complex systems by assembling them from the surfaces and phase regions opens new opportunities in the digitalization of materials science.

The model of the phase diagram, which includes all its topological elements, is a tool for its comprehensive study. It can be used to build iso- and polythermal sections, to calculate crystallization paths and vertical and horizontal mass balances, which allow obtaining complete data on the crystallization stages, the phase and microstructural composition of the sample (without taking into account diffusion processes for each crystallization field), to visualize the results of phase interactions at all crystallization stages, and even to predict the microstructural compositions [99–102] (Fig. 6).

Before constructing a computer 3D model of the phase diagram with the help of the PD Designer program, all components of the system and formed in it compounds were redesignated.

In the case of the TiO_2-Al_2O_3-SiO_2-ZrO_2 quaternary system, the initial oxides were assigned the following letters: A - TiO_2, B - Al_2O_3, C - SiO_2, D - ZrO_2; and their polymorphic modifications were assigned the same letters but with numbers, namely: C – cristobalite (*cr*-SiO_2), C1 – tridymite (*tr*-SiO_2), C2 – high-temperature quartz (HQ-SiO_2) and C3 – low-temperature quartz (LQ-SiO_2); D – cubic (c-ZrO_2) polymorphic modification , D1 – tetragonal (*t*-ZrO_2) polymorphic modification, and D2 – monoclinic (*m*-ZrO_2) polymorphic modification; compounds were indicated with letters R: R1 – Al_2TiO_5, R2 – $ZrTiO_4$, R3 – $ZrSiO_4$, and R4 – $Al_6Si_2O_{13}$.

3.2. A 3D model of the phase diagram of Al_2O_3-SiO_2-ZrO_2

All known information on the Al_2O_3-SiO_2-ZrO_2 (B-C-D) ternary system only concerns the liquidus [69–75], which corresponds to the formation of the $ZrSiO_4$ (R3) zircon by peritectoid reaction (Fig. 2b). This contributes to the determination of the shape of its liquidus surface [69, 70] with the following transformation of its internal field [72–74] (indicated in Fig. 2b as UQ_1E_2).

In addition to the eutectic (E_1, E_2) and quasi-peritectic (Q_1) invariant reactions (Table 1), which we have already mentioned, there is another reaction in the system, described in papers [72-74] as a peritectic or class III reaction [103]. If to consider only the temperature ratios of the invariant points on the liquidus, then this reaction is, indeed, peritectic one:

(1,660 °C): L + SiO_2 + *t*-ZrO_2 → $ZrSiO_4$ ((L+C+D1→R3).

However, it should be taken into account that in the SiO_2-ZrO_2 (C-D) binary system, the eutectic reaction of L → *t*-ZrO_2 + SiO_2 (L→C+D1) at a temperature of 1,687 °C is preceded by the zircon formation in the reaction SiO_2 + *t*-ZrO_2 → $ZrSiO_4$ (C+D1→R3) at 1,676 °C.

Hence, the reaction in a three-component system at a temperature of 1,660 °C cannot be considered peritectic (P) and should be attributed to class II. However, this is a four-phase transformation U: SiO_2 + ZrO_2 → $ZrSiO_4$ + L (C+D→R3+L) and it is not quasi-peritectic (Q). It corresponds to the coexistence of zircon with the melt; therefore, when constructing the 3D model, the corresponding invariant point shall be indicated with the letter U, rather than Q, as was mentioned above.

Despite the fact that the melts formed in the Al_2O_3-SiO_2-ZrO_2 (B-C-D) system at high temperatures are of the greatest practical importance, it is equally important to get an idea of the processes occurring in the solid-phase regions of the system, which is impossible to do without taking into account all polymorphic transitions.

Thus, five more invariant reactions could be expected to occur in the subsolidus, including four eutectoid ones [76].

After the completion of crystallization, three-phase subsolidus regions are formed: Al_2O_3 - *m*-ZrO_2 - $Si_2Al_6O_{13}$ (B-D2-R4), *m*-ZrO_2 - $ZrSiO_4$ - $Si_2Al_6O_{13}$ (D2-R3-R4), and LQ-SiO_2 - $ZrSiO_4$ - $Si_2Al_6O_{13}$ (C3-R3-R4). However, calculations using the NUCLEA database at temperatures above and below 1,054 °C showed that such triangulation is only possible at high temperatures [104]. At lower temperatures (below 1,054°C), triangulation in the subsolidus results in the formation of three other subsystems: Al_2O_3 - *m*-ZrO_2 - $ZrSiO_4$ (B-D2-R3), Al_2O_3 - $ZrSiO_4$ - $Si_2Al_6O_{13}$ (B-R3-R4), and LQ-SiO_2 - $ZrSiO_4$ - $Si_2Al_6O_{13}$ (C3-R3-R4).

Therefore, according to the data on binary systems and the liquidus surfaces of the ternary

system, it should expect six more invariant reactions in the subsolidus, including four eutectoid (E_3-E_6), a quasi-peritectoid (Q_2), and a peritectoid (P) reactions, as shown in the scheme of mono- and invariant states (Table 1) [76, 105, 106].

The tabulated scheme of mono- and invariant states can be converted into a three-dimensional scheme with the help of the PD Designer program [92] (Fig. 3). First, all isothermal planes (simplices) corresponding to invariant reactions are constructed: triangles for E_1-E_6 and P, then, quadrangles for Q_1, Q_2, and U. The directing curves of all ruled surfaces are brought to them (first with straight lines), which results in a 3D scheme of mono- and invariant states, a fragment of which is shown in Fig. 3a. If the surfaces imitating liquidus, solidus, solvus, and transus are constructed on the obtained frame, this gives a prototype of the phase diagram. It consists of 195 surfaces and 72 phase regions. Next, to move to the 3D model of the phase diagram of the real system (Fig. 4b), the base points are moved to the positions specified

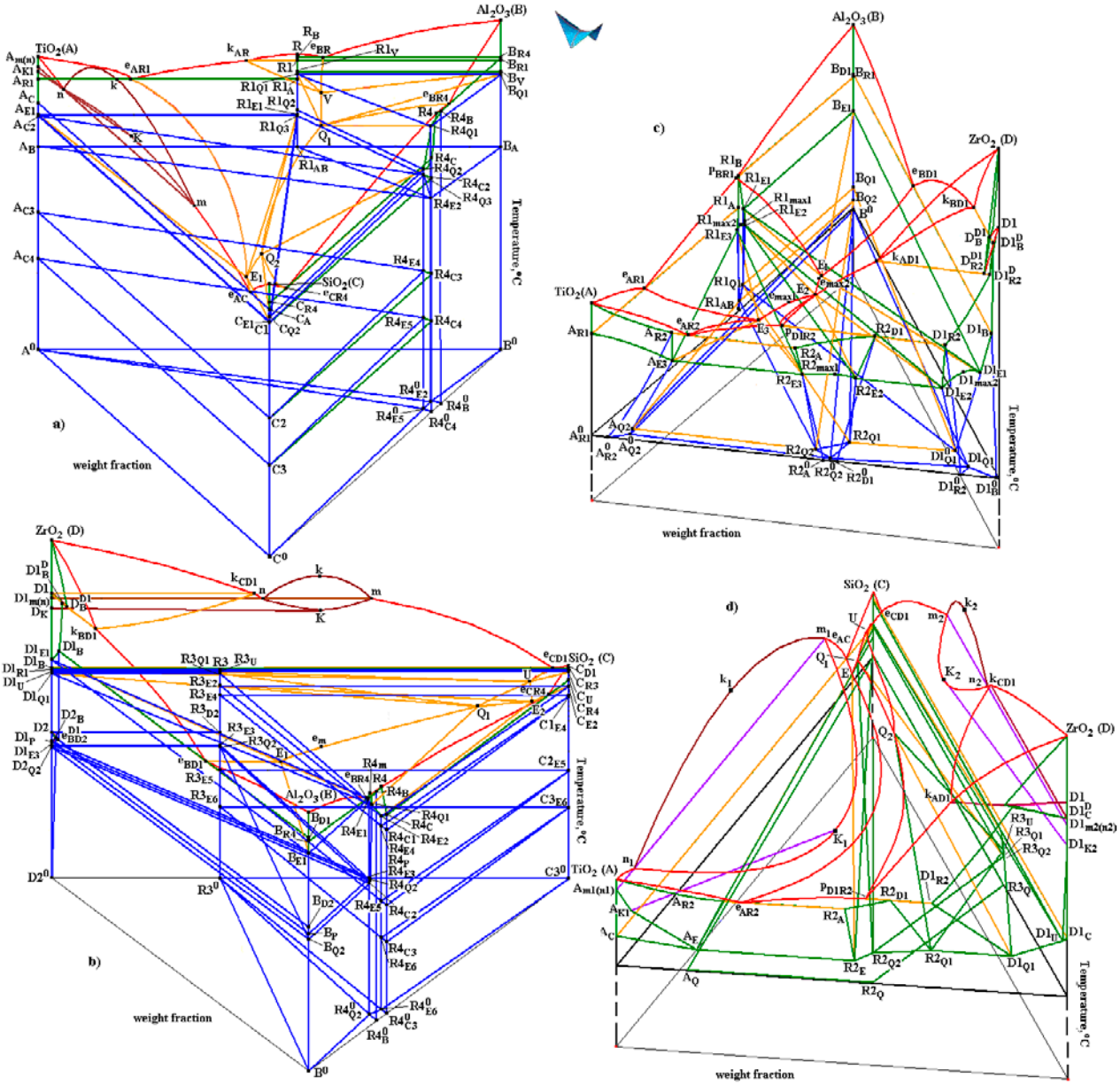

Fig. 4. Computer 3D models of phase diagrams: TiO_2-Al_2O_3-SiO_2 (A-B-C) (a), Al_2O_3-SiO_2-ZrO_2 (B-C-D) (b), TiO_2-Al_2O_3-ZrO_2 (A-B-D) (c) and TiO_2-SiO_2-ZrO_2 (A-C-D) (d), constructed above 1280 °C (c) and 1400 °C (d), correspondingly, with binary compounds Al_2TiO_5 (R1), $ZrTiO_4$ (R2), $ZrSiO_4$ (R3), $Si_2Al_6O_{13}$ (R4)

by real coordinates, and then the curvatures of the lines and surfaces are corrected.

The polythermal sections presented in [88] can be used to assess the quality of the calculations performed with the help of the computer 3D model. However, it should be taken into consideration that they were built at temperatures above 1,500 °C and do not allow evaluating the results of subsolidus modeling.

A comparison of the sections obtained by the 3D model with 14 polythermal sections shown in [88] did not reveal any fundamental discrepancies. However, it be noticed that the shape of the lines that form as a result of the intersection of the vertical plane with the ruled boundaries of three-phase regions (for example, at the boundaries of the L1+L2+D1 region indicated in Fig. 5b as 2L+Tss) is unacceptable for the sections of ruled surfaces. In addition, the regions of limited solubility of the components and zircon (R3) in the polymorphic modifications of ZrO_2 are so small in the 3D model that, unlike [88], they are not visible in the polythermal section S(0, 0.9, 0.1)-ZrO_2 (Fig. 5a). However, in contrast to [88], two-phase regions of mullite (R4) with all four modifications of SiO_2 (C) appear in this section.

The 3D model of the phase diagram of the ZrO_2-SiO_2-Al_2O_3 system was used to calculate the vertical diagrams of material balances for a given center of mass in the entire range of temperatures (Fig. 6a, Table 2).

For example, the crystallization of the G(0.34, 0.46, 0.20) melt proceeded through the following stages:

– Separation of primary crystals of *t*-ZrO_2 (D1) in the range from 1,896.9 to 1,677 °C.

– Eutectic crystallization of *t*-ZrO_2 and $Al_6Si_2O_{13}$ (R4) mullite within the range of 1,677-1,645 °C.

– Quasi-peritectic invariant reaction Q_1 at 1,645 °C: L+D1→R3+R4.

– Eutectic separation of mullite and zircon in the range of 1,645-1,550 °C, transitioning to the eutectic invariant transformation E_2 at 1,550 °C together with SiO_2 (C). This was followed by three polymorphic eutectoid transformations between SiO_2 modifications at temperatures of 1,470, 867, and 573 °C, respectively (Table 2). The same stages of crystallization were confirmed by the calculation of phase trajectories (Fig. 6b), where the crystallization path for the center of mass G is shown by the green line.

3.3. A 3D model of the phase diagram of TiO_2-Al_2O_3-SiO_2

Earlier, a simplified 3D model of the phase diagram of the TiO_2-Al_2O_3-SiO_2 (A-B-C) system was developed with congruently melting aluminum titanate. This model only included the high-temperature part (above 1,470 °C) of the phase diagram [107].

If the version of the TiO_2-Al_2O_3 phase diagram which does not take into account the formation of the $Al_6Ti_2O_{13}$ compound, but does take into account the polymorphism of $AlTiO_5$ is taken as the basis, then its high-temperature polymorphic modification shall be assigned with the designation R, its low-temperature polymorphic modification shall be indicated as R1, and the $Al_6Si_2O_{13}$ mullite as R4 (Fig. 4a).

There are an eutectic reaction between silicon and titanium oxides. The liquid immiscibility

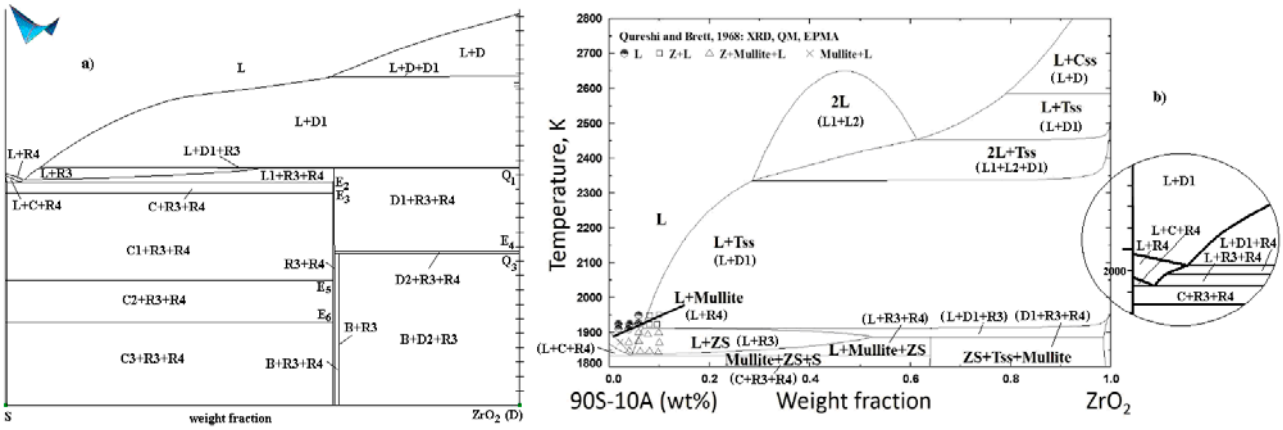

Fig. 5. Polythermal section S(0.1, 0.9, 0)-ZrO_2 (D): of the 3D model (a), calculated by CALPHAD-technology [88] (b)

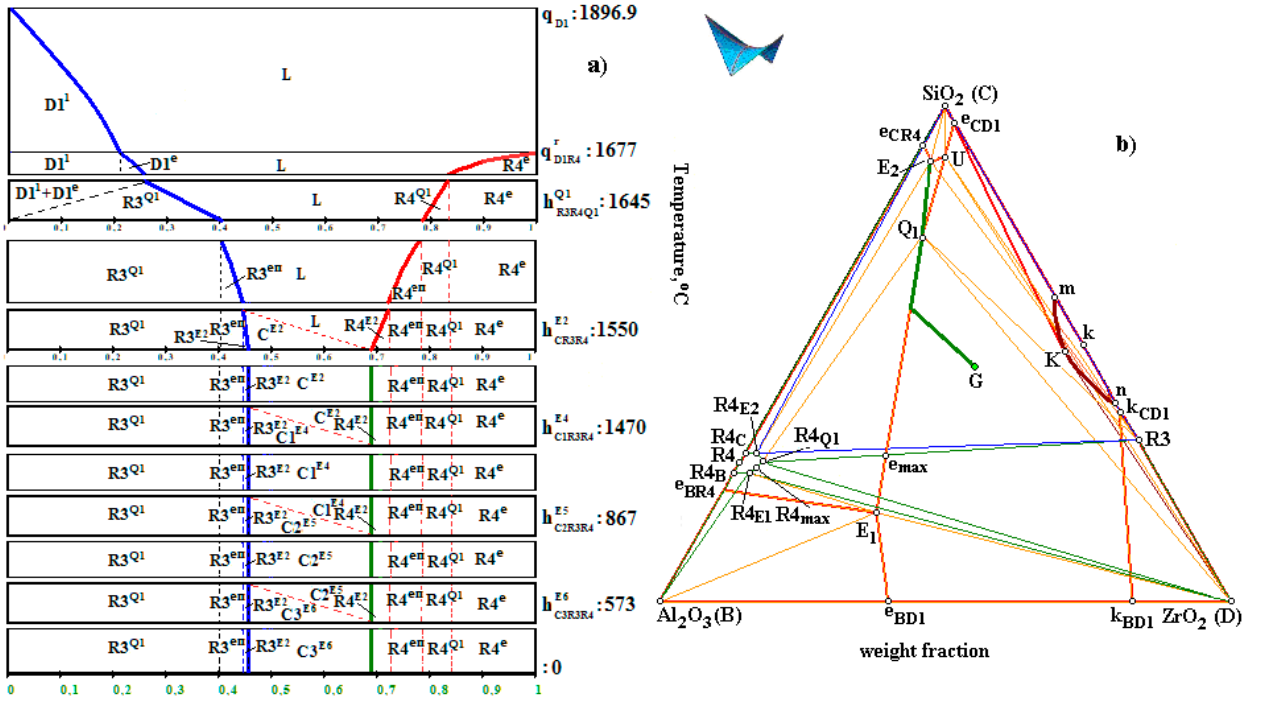

Fig. 6. Mass balance diagram showing the change in the phase composition of the melt G(0.34, 0.46, 0.20) during its crystallization in the Al_2O_3-SiO_2-ZrO_2 (B-C-D) system (a) and the melt path (b) (temperature °C, compositions – wt. fractions)

Table 2. Calculation of mass fractions of phases during crystallization of melt G(0.34, 0.46, 0.20) in the Al_2O_3-SiO_2-ZrO_2 (B-C-D) system (Fig. 6) until the end of the E_2 reaction (temperature °C, compositions - wt. fractions)*

Phase region	*T*, °C	Mass fractions of phases
L+D1	1896.9	L=1, D1=0
(L→$D1^1$)	1677	L=0.758, $D1^1$=0.242
L+D1+R4	1677	L=0.758, $D1^1$=0.242, R4=0
(L→$D1^e$+$R4^e$)	1645	L=0.563, D1($D1^1$=0.242, $D1^e$=0.042)=0.284, $R4^e$=0.153
L+D1→$R3^{Q1}$+$R4^{Q1}$	1645	L=0.563, D1($D1^1$=0.242, $D1^e$=0.042)=0.284, $R4^e$=0.153, R3=0 L=0.345, D1=0, $R3^{Q1}$=0.447, R4($R4^e$=0.153, $R4^{Q1}$=0.055)=0.208
L+R3+R4	1645	L=0.345, $R3^{Q1}$=0.447, R4($R4^e$=0.153, $R4^{Q1}$=0.055)=0.208;
(L→$R3^{en}$+$R4^{en}$)	1550	L=0.249, R3($R3^{Q1}$=0.447, $R3^{en}$=0.039)=0.486; R4($R4^e$=0.153, $R4^{Q1}$=0.055, $R4^{en}$=0.057)=0.265
L→C^{E2}+$R3^{E2}$+$R4^{E2}$	1550	L=0.249, R3($R3^{Q1}$=0.447, $R3^{en}$=0.039)=0.486; R4($R4^e$=0.153, $R4^{Q1}$=0.055, $R4^{en}$=0.057)=0.265; C=0 L=0; R3($R3^{Q1}$=0.447, $R3^{en}$=0.039, $R3^{E2}$=0.01)=0.496; R4($R4^e$=0.153, $R4^{Q1}$=0.055, $R4^{en}$=0.057, $R4^{E2}$=0.029)=0.294; C^{E2}=0.210

*1 – primary crystallization;
e – univariant eutectic crystallization;
ep – post-peritectic univariant crystallization;
Q – invariant quasi-peritectic mass regrouping;
E – invariant eutectic (eutectoid) crystallization

L1 → L2 + TiO_2 (L1→L2+A) in the TiO_2-SiO_2 (A-C) binary system is appeared in the form of a small mknK cupola on the TiO_2 liquidus surface in the TiO_2-Al_2O_3-SiO_2 (A-B-C) ternary system. It only affectes the geometry of the solidus surface of titanium oxide in the form of the $A_{m(n)}A_K$ fold conjugated with the line of the intersection of the immiscibility cupola with this liquidus surface.

Since the congruently melting Al_2TiO_5 (R1) aluminum titanate devides the TiO_2-Al_2O_3 (A-B)

binary system into two subsystems: TiO_2-Al_2TiO_5 (A-R1) and Al_2TiO_5-Al_2O_3 (R1-B), the high-temperature modification R has two liquidus branches extending both into the subsystem with TiO_2 (liquidus cuver Rk_{AR}) and into the subsystem with Al_2O_3 (cuver Re_{BR}) (Fig. 4a).

Importantly, the polymorphism of Al_2TiO_5 manifestes itself differently in the subsystems. In the TiO_2-Al_2TiO_5 (A-R1) subsystem, it has the form of the R→R1+L metatectic reaction, as a result the liquidus in this subsystem consists of three branches corresponding to the onset primary crystallization of TiO_2 (A) (cuver Ae_{AR1}) and of compounds R (cuver Rk_{AR}) and R1 (cuver $k_{AR}e_{AR1}$) (Fig. 4a). In the Al_2TiO_5-Al_2O_3 (R1-B) subsystem, the liquidus has two branches: the onset primary crystallization of Al_2O_3 (B) (cuver Be_{BR}) and of R (cuver Re_{BR}). The polymorphic transition occurres below the liquidus by the R→R1+B eutectoid reaction.

Another feature of aluminum titanate is its decomposition into initial oxides at 1,300 °C [51].

In the Al_2O_3-SiO_2 (B-C) system, the $Al_6Si_2O_{13}$ (R4) mullite devides the system into two eutectic subsystems: Al_2O_3-$Al_6Si_2O_{13}$ (B-R4) and $Al_6Si_2O_{13}$-SiO_2 (R4-C).

Both binary systems with silicon oxide are differed by polymorphic transitions between the four modifications of silicon oxide (C). Polymorphic transitions are degenerated and their type are not clear. The 3D model suggests that eutectoid transformations took place. In the system constituting TiO_2 (A), they occurres with the participation of titanium oxide (A): C→C1+A, C1→C2+A, C2→C3+A, while in the system with Al_2O_3 (B), it occurres with the participation of mullite (R4): C→C1+R4, C1→C2+R4, C2→C3+R4.

To proceed with the 3D model, it are necessary to understand the structure of the phase diagram in the subsolidus. After the Q_1, Q_2, E_1 reactions completed (see section 2.2 and Fig. 2a), there are three ternary subsystems: B-R1-R4 (after Q_1), C-R1-R4 (after Q_2), and A-R1-C (after E_1). However, after completion of the eutectic reaction E_1, further solid-phase transformations takes place. First, there are three polymorphic transitions of silicon oxide. Secondly, in the TiO_2-Al_2O_3 (A-B) binary system, the low-temperature polymorphic modification of aluminum titanate (R1) decomposes into the initial oxides, TiO_2 and Al_2O_3. Naturally, the decomposition of R1 are also expected in the ternary system.

Earlier, the authors of [105] represented the following rearrangement in the Al_2O_3-SiO_2-ZrO_2 (B-C-D) system: in the B-R3-R4-D subsystem, the stable diagonal D-R4 replaced the diagonal B-R3. A similar situation are in the TiO_2-Al_2O_3-SiO_2 (A-B-C) system: after the completion of the Q_2 and E_1 reactions, the A-R1-R4-C subsystem has a stable diagonal C-R1. Therefore, there is a high probability of a rearrangement with stable diagonal A-R4 due to the invariant transformation of the quasiperitectoid type Q_3: C+R1→A+R4. This can be explained by the fact that in all variants of the binary system (Fig. 4), aluminum titanate R1 decomposes into TiO_2 (A) and Al_2O_3 (B). Therefore, if conditions for its decomposition are created in a ternary system, we should expect such a triangulation on the the A-R1-R4 and B-R1-R4 subsystems and the subsequent disappearance of the R1-R4 diagonal. Therefore, after the completion of the Q_3 reaction (rearrangement), the subsolidus should be presented by three subsystems: B-R1-R4 (after Q_1), A-R1-R4, and A-C-R4. Further, the R1-R4 segment separating the A-R1-R4 and B-R1-R4 subsystems should disappear. This should occur after the decomposition of R1 into A and B (in the presence of R4) by the reaction E_2: R1→A+B+R4.

In confirmation of this fact, a reaction was experimentally determed at 1469.85 °C in work [68]:

Q_3: $SiO_2 + Al_2TiO_5 \rightarrow TiO_2 + Al_6Si_2O_{13}$
(C+R1→A+R4),

which indicates rearrangement from the C+R1 diagonal to the A+R4 diagonal. In [67], studies in the subsolidus region showed that at 1,470–1,300°C (i.e. within the interval between the reactions Q_3 and E_2), two phase regions are formed: $TiO_2 + SiO_2 + Al_6Si_2O_{13}$ (A+C+R4) and $TiO_2 + Al_2TiO_5 + Al_6Si_2O_{13}$ (A+R1+R4).

In the TiO_2-Al_2O_3 (A-B) binary system, the decomposition of aluminum titanate (R1) occurs at 1,300 °C and zero mutual solubility of both initial oxides, while in the ternary system, the decomposition E_2: R1→A+B+R4 should occur at the same temperature of 1,300 °C. Therefore, the Q_3 rearrangement can be expected in the temperature range of $T_{E2} < T < T_{E1}$. The

temperature indicated in [68] is 1,470 °C / 1,743 K.

After the R1 decomposition by the E_2 reaction, crystallization in the A-B-R4 subsystem is completed. In the second subsystem A-C-R4, the set of polymorphic transitions E_3: C→C1+A+R4, E_4: C1→C2+A+R4, E_5: C2→C3+A+R4 are followed the after Q_3 rearrangement.

Thus, a 3D model of the TiO_2-Al_2O_3-SiO_2 (A-B-C) phase diagram is formed and consisted of 173 surfaces and 64 phase regions (Fig. 4a).

When constructing the 3D model, the following data on the structure of binary systems were used: the TiO_2-SiO_2 system [18], the TiO_2-Al_2O_3 system [51], and the Al_2O_3-SiO_2 system [29]. For the ternary system, we used liquidus data published in [68]. The choice was due to the fact that these data were obtained experimentally and contained the most complete information about the structure of the phase diagrams of binary systems, liquidus surfaces, and possible transformations in the subsolidus.

Model sections and obtained in [68] are compared for validation of the 3D model. These sections are well matched, which confirmed the correctness of the constructed model.

3.4. 3D models of phase diagrams of TiO_2-Al_2O_3-ZrO_2 and TiO_2-SiO_2-ZrO_2

When constructing 3D models of phase diagrams of ternary systems based on the TiO_2-ZrO_2 (A-D) binary system with the addition of Al_2O_3 (B) (Fig. 4c) and SiO_2 (Fig. 4d), we used the interpretation of the TiO_2-Al_2O_3 (A-B) binary system, according to which aluminum titanate polymorphism was not taken into account and the type of its melting was understood as being incongruent (Fig. 1f). This version was accepted in one of the recent works [51], but experimental work in this area continues. Nevertheless, the missing data are not an obstacle to constructing a 3D model, because the possible future adjustment of the type of aluminum titanate melting will not require significant changes in the geometry of the phase diagram. And even if the polymorphism of Al_2TiO_5 (R1) is confirmed, according to [52], its liquidus field will have to be divided into two fragments, which will not significantly affect the 3D model as a whole and will only affect a few fragments of the "upper" temperature part of the phase diagram.

According to [77], there are three eutectic transformations on the liquidus in the system with aluminum oxide (Fig. 2c):

E_1 (1,705 °C): $L \rightarrow Al_2O_3 + t\text{-}ZrO_2 + Al_2TiO_5$ (L→B+D1+R1),

E_2 (1654 °C): $L \rightarrow t\text{-}ZrO_2 + Al_2TiO_5 + ZrTiO_4$ (L→D1+R1+R2),

E_3 (1636 °C): $L \rightarrow TiO_2 + Al_2TiO_5 + ZrTiO_4$ (L→A+R1+R2),

There are also rearrangements in the subsolidus:

Q_1 (1,375 °C): $t\text{-}ZrO_2 + Al_2TiO_5 \rightarrow Al_2O_3 + ZrTiO_4$ (D1+R1→B+R2),

Q_2 (1,320 °C): $Al_2TiO_5 + ZrTiO_4 \rightarrow TiO_2 + Al_2O_3$ (R1+R2→A+B).

After eutectic transformations, the system is triangulated into three subsystems:

TiO_2 - Al_2TiO_5 - $ZrTiO_4$ (A-R1-R2),
t-ZrO_2 - Al_2TiO_5 - $ZrTiO_4$ (D1-R1-R2),
Al_2O_3 - t-ZrO_2 - Al_2TiO_5 (B-D1-R1).

At the stage of the first rearrangement, as a result of reaction Q_1, the stable diagonal ZrO_2-Al_2TiO_5 (D1-R1) is replaced by Al_2O_3+$ZrTiO_4$ (B-R2). The second rearrangement result is the decomposition of aluminum titanate (R1) into TiO_2 and Al_2O_3 (A and B) and the system being divided into two subsystems: TiO_2 - Al_2O_3 - $ZrTiO_4$ (or A-B-R2), Al_2O_3 - t-ZrO_2 - $ZrTiO_4$ (B-D1-R2).

When constructing a computer 3D model of the phase diagram of the TiO_2-Al_2O_3-ZrO_2 system, we took into account the experimental and calculated data on the structure of binary systems and primary crystallization surfaces published in [2, 6–7, 49, 51, 77].

The coordinates of ternary eutectic reactions (E_1, E_2) were determined experimentally in [77]. The temperatures of the invariant transformations Q_1 and Q_2 in the subsolidus were also presented. (The coordinates of the maximum points on the invariant liquidus lines were only obtained by calculation in [77], and they were set approximately in the 3D model).

As a result, the computer 3D model of the phase diagram fragment limited from below by the temperature of 1,280 °C is formed by 77 surfaces and 27 phase regions.

The 3D model of the TiO_2-SiO_2-ZrO_2 (A-C-D) phase diagram is limited to a temperature of

1,400 °C, since isothermal sections at temperatures of 1,400 and 1,500 °C are described in [82] and only this limited information can be used to assess the quality of the obtained 3D model.

Two regions of liquid immiscibility on the side of binary systems with silicon oxide are two cupolas located on the surfaces of the onset crystallization of TiO_2 and the tetragonal form of ZrO_2, respectively (Fig. 2d). In addition to the primary crystallization fields of the cubic form of ZrO_2, SiO_2, and zirconium titanate ($e_{AR2}EQ_2Q_1p_{D1R2}$), the internal field of zircon (Q_1Q_2U) appears on the liquidus.

In total, four invariant reactions with the participation of the melt take place in the system, including two quasiperitectic reactions and one eutectic reaction:

Q_1 (1,575 °C): L + *t*-ZrO_2 → $ZrTiO_4$ + $ZrSiO_4$ (L+D1→R2+R3),

Q_2 (1,545 °C): L + $ZrSiO_4$ → SiO_2 + $ZrTiO_4$ (L+R3→C+R2),

E (1,500 °C): L → TiO_2 + SiO_2 + $ZrTiO_4$ (L→A+C+R2).

As mentioned above the 3D model was constructed according to the data provided in [82], in which the temperature of the invariant peritectic reaction P: L + SiO_2 + *t*-ZrO_2 ZrSiO→ $ZrSiO_4$ (L+C+D1→R3) was indicated as 1,670 °C, while the temperature of the SiO_2 + *t*-ZrO_2 → $ZrSiO_4$ (C+D1→R3) zircon formation, according to the data in [1], was 1,676 °C, which was higher than the temperature of the ternary peritectic reaction. Then, one of the following is possible: either the invariant reaction in the ternary system is not peritectic, or zircon decomposes at a temperature lower than 1,670 °C.

When we constructed the 3D model, we assumed that the invariant reaction named in [82] as peritectic was actually not peritectic. Technically, this reaction could be considered as peritectic according to the reduction in temperature on the invariant liquidus lines (Fig. 2d), however, since this reaction was preceded the zircon formation at 1,676 °C, along with binary eutectic reaction e_{CD1}: L → SiO_2 + *t*-ZrO_2 (L→C+D1) at 1,687 °C, this invariant reaction at 1,670 °C can be presents as follows

U: SiO_2 + t-ZrO_2 → $ZrSiO_4$ + L (C+D1→R3+L),

which also corresponds to the formation of zircon, but in the presence of melt L. Since there is no unified terminology for invariant reactions, this reaction is indicated with letter U in the 3D model.

Therefore, a three-phase region ZrO_2 + $ZrTiO_4$ + $ZrSiO_4$ (D1+R2+R3) is formed in the ternary system after the quasi-peritectic reaction Q_1 below 1,575 °C. In the TiO_2-SiO_2-$ZrSiO_4$-$ZrTiO_4$ (A-C-R3-R2) subsystem, initially divided by the diagonal SiO_2-$ZrTiO_4$ (C-R2) [82], the rearrangement SiO_2 + $ZrTiO_4$ → TiO_2 + $ZrSiO_4$ (C+R2→A+R3) is predicted.

Further studies of the TiO_2-ZrO_2 (A-D) binary system in the subsolidus are needed to draw conclusions about phase transformations in the rest of the concentration space of the phase diagram after the rearrangement at temperatures below 1,400 °C.

Hence, the 3D model of a fragment of the phase diagram is assembled from 67 surfaces and 26 phase regions.

The projection of the liquidus surfaces presented in [82] does not take into account an immiscibility region on the side of the ZrO_2-SiO_2 binary system and the liquidus surface corresponding to the cubic modification of c-ZrO_2 either. Therefore, to form the immiscibility surface, we added a binary monotectic line at 2,250 °C in the range of 41–62 wt. % of SiO_2 and the upper critical point at 2,430 °C and 53 wt. % SiO_2 according to [23].

The 3D model of the phase diagram took into account the configuration and curvature of the liquidus surfaces and the immiscibility surface on the side of the TiO_2-SiO_2 binary system. The corresponding immiscibility surface in the crystallization field of TiO_2 occupies a significant area and its projection extendes to the middle of the triangle of compositions. When modeling the liquidus surface corresponding to the primary crystallization of zircon, the *s*-shape of the liquidus line at the boundary of the zircon field and the tetragonal form of ZrO_2 was taken into account. In addition, the 3D model specified the immiscibility surface adjacent to the SiO_2-ZrO_2 binary system and the surface of the primary crystallization of the cubic form of ZrO_2, which were not previously cosiderated in [82].

4. A 4D model of the isobaric phase diagram of the TiO_2-Al_2O_3-SiO_2-ZrO_2 quaternary system and prediction of the geometric structure of its high-temperature part

The data on invariant transformations in the boundaring systems was used to propose the scheme of phase reactions for the TiO_2-Al_2O_3-SiO_2-ZrO_2 quaternary system (Table 3) [108]. The system is symmetrical and consists of two parts, each of which includes a peritectic π, a quasi-peritectic μ, and a eutectic ε reactions. The main difference in these reactions is the participation of either mullite or zirconium titanate. Zircon is formed in both peritectic reactions, while in quasi-peritectic transformations crystallization of either of zirconium titanate (in μ_2) or tetragonal polymorphic modification of zirconium oxide (in μ_1) is completed.

After the completion of eutectic reactions, tetrahedration results in four subsystems (Fig. 7):

TiO_2 - SiO_2 - Al_2TiO_2 - $ZrTiO_4$ (A-C-R1-R2) after ε_2 at T < 1,470 °C,

SiO_2 - t-ZrO_2 - Al_2TiO_2 - $ZrTiO_4$ (C-D1-R1-R2) after μ_2,

SiO_2 - t-ZrO_2 - Al_2TiO_2 - $Al_6Si_2O_{13}$ (C-D1-R1-R4) after μ_1,

Al_2O_3-(t-ZrO_2)-Al_2TiO_2-$Al_6Si_2O_{13}$ (B-D1-R1-R4) after ε_1 at T < 1,480 °C.

This scheme can be used to describe the contours of ten liquidus hypersurfaces and ten solidus hypersurfaces (the zircon liquidus consists of two fragments). Immiscibility of liquid, which takes place in the TiO_2-SiO_2 and SiO_2-ZrO_2 binary systems both within the corresponding ternary and quaternary systems, remains independent and does not affect in any way the overall geometric configuration of the phase diagram of the quaternary system, or the phase transformations in this system. In addition, according to the scheme, 19 three-phase regions with the participation of the melt have been formed in the system (with due account of two regions of liquid immiscibility, L1+L2 + TiO_2 and L1 + L2+Al_2O_3) and 18 similar four-phase regions.

5. Conclusion

For the TiO_2-Al_2O_3-SiO_2 system, a total of eight variants of the liquidus structure are possible. They differ in the type melting (congruent or incongruent) of both mullite and aluminum titanate, the presence or absence of its polymorphism, and the possibility of the formation of one more compound, $Al_6Ti_2O_{13}$.

A three-dimensional computer model for one of the variants, i.e. congruently melting mullite and aluminum titanate with two polymorphic modifications has been designed. This model can be easily transformed into any of the seven

Table 3. The scheme of phase reactions with the melt participation in the TiO_2-Al_2O_3-SiO_2-ZrO_2 system*

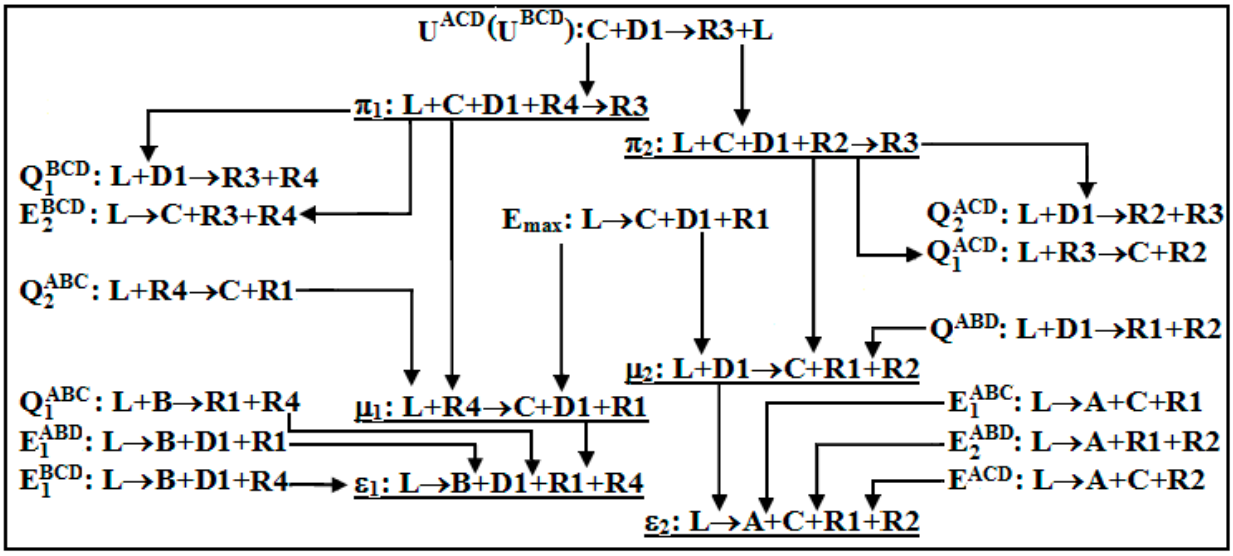

* Initial oxides are designated as: TiO_2 – A, Al_2O_3 – B, SiO_2 – C, c-ZrO_2 – D, t-ZrO_2 – D1, compounds – Al_2TiO_5 – R1, $ZrTiO_4$ – R2, $ZrSiO_4$ – R3, $Al_6Si_2O_{13}$ – R4

The superscripts indicate the invariant points of the corresponding ternary systems

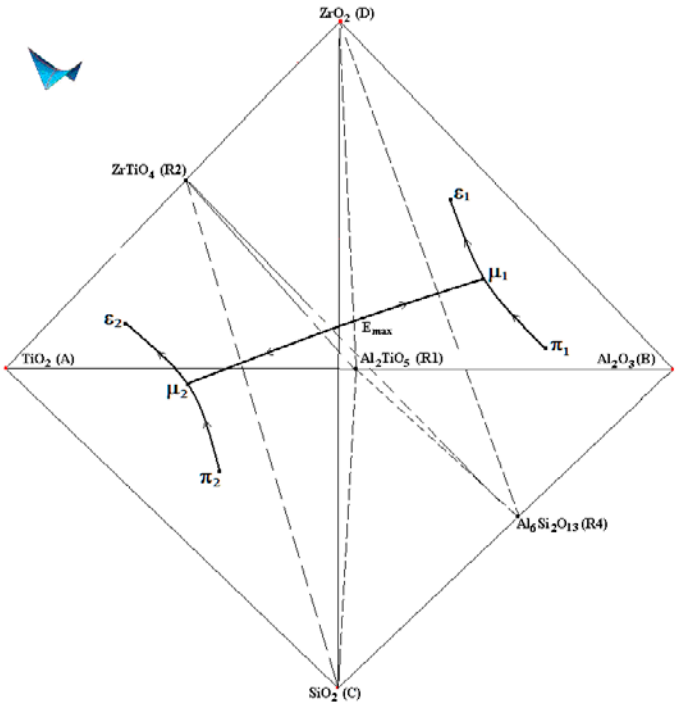

Fig. 7. Tetrahedration scheme of the TiO_2-Al_2O_3-SiO_2-ZrO_2 system with compounds Al_2TiO_5 (R1), $ZrTiO_4$ (R2), $Al_6Si_2O_{13}$ (R4) after eutectic reactions ending and drawing of univariant liquidus lines connecting quaternary invariant points

other variants should new refined experimental data appear.

Since there is no definitive description of the phase transformations in the TiO_2-ZrO_2 system, the modeling of two ternary systems formed on its basis is limited by the temperatures of aluminum titanate decomposition:

– 1,280 °C, which was used to construct four variants of the TiO_2-Al_2O_3-ZrO_2 phase diagram (which is due to the presence of four versions of the TiO_2-Al_2O_3 phase diagram). The quality of the 3D models can be assessed by comparing them with the isothermal sections described in previous studies [77].

– 1,400 °C, which was used for both versions of the 3D model of the TiO_2-SiO_2-ZrO_2 phase diagram (built in the assumption that zircon is formed by either a peritectic or a peritectoid reaction). In this case, it is possible to compare the model sections at 1,400 and 1,500 °C with previously published data [82].

Of the four possible variants of the Al_2O_3-SiO_2-ZrO_2 phase diagrams, which differ in the type melting of mullite and zircon, two variants of 3D models were constructed: when mullite melts congruently, zircon can be formed either by a peritectic or by a peritectoid reaction.

In general, the 3D models of the phase diagrams of the considered ternary systems, after minor adjustments that may be required when new, clarifying information is received, can be used in practice.

For the TiO_2-Al_2O_3-SiO_2-ZrO_2 four-component system, a scheme of phase reactions with the participation of the melt was deduced, which includes six five-phase invariant reactions: two peritectic, two eutectic, and two quasi-peritectic reactions.

It was assumed that its liquidus consists of 12 hypersurfaces, of which two correspond to the regions of immiscibility of liquid, while the remaining ten correspond to the onset primary crystallization of the initial oxides, including two high-temperature polymorphic modifications of zirconium oxide, two congruently melting compounds (aluminum titanate and mullite), incongruently melting zirconium titanate, and two fragments of the liquidus hypersurfaces of zircon.

The resulting prototype of the liquidus of the four-component oxide system will be used for the planning of further experiments, first of all, aimed at determining the coordinates of the estimated six invariant points.

Contribution of the authors

The authors contributed equally to this article.

Conflict of interests

The authors declare that they have no known competing financial interests or personal relationships that could have influenced the work reported in this paper.

References

1. Butterman W. C., Foster W. R. Zircon stability and the ZrO_2-SiO_2 phase diagram. *American Mineralogist*. 1967;52(5-6): 880–885.

2. Lakiza S. M., Lopato L. M. Stable and metastable phase relations in the system alumina-zirconia-yttria. *Journal of the American Ceramic Society*. 1997;80(4): 893–902. https://doi.org/10.1111/j.1151-2916.1997.tb02919.x

3. Fedorov P. P., Yarotskaya E. G. Zirconium dioxide. Review. *Condensed Matter and Interphases*. 2021;23(2): 169–187. https://doi.org/10.17308/kcmf.2021.23/3427

4. Fischer G. R., Manfredo L. J., McNally R. N., Doman R. C. The eutectic and liquidus in the Al_2O_3-ZrO_2 system. *Journal of Materials Science*. 1981;16: 3447–3451. https://doi.org/10.1007/BF00586307

5. Jerebtsov D. A., Mikhailov G. G., Sverdina S. V. Phase diagram of the system: Al_2O_3–ZrO_2. *Ceramics International*. 2000;26: 821. https://doi.org/10.1016/S0272-8842(00)00023-7

6. Lakiza S., Fabrichnayay O., Wang Ch., Zinkevich M., Aldinger F. Phase diagram of the ZrO_2-Gd_2O_3-Al_2O_3 system. *Journal of the American Ceramic Society*. 2006;26: 233–246. https://doi.org/10.1016/j.jeurceramsoc.2004.11.011

7. Fabrichnaya O., Aldinger F. Assessment of thermodynamic parameters in the system ZrO_2-Y_2O_3-Al_2O_3. *International Journal of Materials Research*. 2004;95: 27–39. https://doi.org/10.3139/146.017909

8. Bunting E. N. Phase equilibria in the systems TiO_2, TiO_2-SiO_2 and TiO_2-Al_2O_3. *Bureau of Standards Journal of Research*. 1933;11: 719–725. https://doi.org/10.6028/jres.011.049

9. Toropov N. A., Barzakovskii V. P., Lapin V. V., Kurtseva N. N. *State diagrams of silicate systems. The handbook. Part 1: binary systems*[*]. Leningrad: Nauka Publ.; 1969. 822 p. (In Russ.)

10. Umezu S., Kakiuchi F. Investigations on iron blast. Furnace slags containing titanium. *Nippon Kogyo Kwaishi*. 1930;46: 866–877.

11. DeVries R. C., Roy R., Osborn E. F. The system TiO_2-SiO_2. *Transactions of the British Ceramic Society*. 1954;53 (9): 525–540.

12. Morey G. W. *Data of geochemistry. Chapter L. Phase-equilibrium relations of the common rock-forming oxides except water*. Washington: United States Government Printing Office; 1964. 146 p. https://doi.org/10.3133/pp440l

13. McTaggart G. D., Andrews A. I. Immiscibility area in the system TiO_2-ZrO_2-SiO_2. *Journal of the American Ceramic Society*. 1957;40(5): 167–170. https://doi.org/10.1111/j.1151-2916.1957.tb12596.x

14. Galakhov F. Ya., Areshev M. P., Vavilonova V. T., Aver'yanov V. I. Determination of the boundaries of metastable liquation in the silica part of the TiO_2-SiO_2 system[*]. *Izvestiia Akademii nauk SSSR: Neorganicheskie materialy*. 1974;10(1): 179–180. (In Russ.)

15. Kamaev D. N., Archugov S. A., Mikhailov G. G. Experimental study and thermodynamic modeling of the TiO_2-SiO_2 system[*]. In: *Computer modeling of the physicochemical properties of glasses and melts: Proc. VIII Rus. seminar, 16–19 October 2006*. Kurgan: Kurgan State University; 2006. p. 35–36. (In Russ.)

16. DeCapitani C., Kirschen M. A Generalized multicomponent excess function with application to immiscible liquids in the system CaO-SiO_2-TiO_2. *Geochimica et Cosmochimica Acta*. 1998;62 (23/24): 3753–3763. https://doi.org/10.1016/S0016-7037(98)00319-6

17. Kirschen M., DeCapitani C., Millot F., Rifflet J.-C., Coutures J.-P. Immiscible silicate liquids in the system SiO_2-TiO_2-Al_2O_3. *European Journal of Mineralogy*. 1999;11(3): 427–440. https://doi.org/10.1127/ejm/11/3/0427

18. Kirillova S. A., Almjashev V. I., Gusarov V. V. Spinodal decomposition in the SiO_2-TiO_2 system and hierarchically organized nanostructures formation. *Nanosystems: Physics, Chemistry, Mathematics*. 2012;3(2): 100–115. (In Russ.). Available at: https://nanojournal.ifmo.ru/files/volume7/10Almjashev.pdf

19. Kirillova S. A., Almjashev V. I., Gusarov V. V. Phase Relationships in the SiO_2-TiO_2 System. *Russian Journal of Inorganic Chemystry*. 2011;56 (9): 1464–1471. 10.1134/S0036023611090117.

20. Boulay E., Nakano J., Turner S., Idrissi H., Schryvers D., Godet S. Critical assessments and thermodynamic modeling of BaO-SiO_2 and SiO_2-TiO_2 systems and their extensions into liquid immiscibility in the BaO-SiO_2-TiO_2 system. *CALPHAD*. 2014;47: 68–82. https://doi.org/10.1016/j.calphad.2014.06.004

21. Ilatovskaia M., Fabrichnaya O. Liquid immiscibility and thermodynamic assessment of the Al_2O_3-TiO_2-SiO_2 system. *Journal of Phase Equilibria and Diffusion*. 2022;43: 15–31. https://doi.org/10.1007/s11669-021-00935-4

22. Geller R. F., Lang S. M. System SiO_2-ZrO_2. Journal of the American Ceramic Society. 1949;32: 157–159.

23. Toropov N. A., Galakhov F. Ya. Liquation in ZrO_2-SiO_2 system. *Bulletin of the Academy of Sciences of the USSR*. 1956;(2): 153–162. https://doi.org/10.1007/BF01177636

24. Berezhnoi A. S. *Multicomponent systems of oxides*. Kiev: Naukova Dumka Pulb.; 1970. 542 p. (In Russ.)

25. Kwon S. Y., Jung I.-H. Critical evaluation and thermodynamic optimization of the CaO-ZrO_2 and SiO_2-ZrO_2 systems. *Journal of the European* Ceramic *Society*. 2017;37(3): 1105–1116. https://doi.org/10.1016/j.jeurceramsoc.2016.10.008

26. Kamaev D. N., Archugov S. A., Mikhailov G. G. Study and thermodynamic analysis of the ZrO_2-SiO_2 system. *Russian Journal of Applied Chemistry*. 2005;78: 200–203. https://doi.org/10.1007/s11167-005-0259-2

27. Björkvall J., Stolyarova V. L. A mass spectrometric study of Al_2O_3-SiO_2 melts using a Knudsen cell. *Rapid Communications in Mass Spectrometry*. 2001;15: 836–842. https://doi.org/10.1002/rcm.251

28. Bowen N. L., Greig J. W. The system Al_2O_3-SiO_2. *Journal of the American Ceramic Society*. 1924;7(4): 238–254. https://doi.org/10.1111/j.1151-2916.1924.tb18190.x

29. Toropov N. A., Galakhov F. Ya. Solid solutions in the Al_2O_3-SiO_2 system. *Bulletin of the Academy of Sciences of the USSR Division of Chemical Science*. 1958;7(1): 5–9. https://doi.org/10.1007/BF01170853

30. Aramaki S., Roy R. Phase diagram for the system Al_2O_3-SiO_2. *Journal of the American Ceramic Society*. 1962;45(5): 229–242. https://doi.org/10.1111/j.1151-2916.1962.tb11133.x

31. Levin E. M., Robbins C. R., McMurdie H. F. *Phase diagrams for ceramists*. Ohio: American Ceramic Society; 1964. 600 p.

32. *Atlas of slags*[*]. Ref. book: trans. with him. I. S. Kulikova (ed.). Moscow: Metallurgy Publ.; 1985. 208 p. (In Russ.)

33. Strelov K. K., Kashcheev I. D. Phase diagram of the system Al_2O_3-SiO_2. *Refractories*. 1995;36 (7-8): 244–246. https://doi.org/10.1007/BF02227394

34. Fabrichnaya O., Costa e Silva A., Aldinger F. Assessment of thermodynamic functions in the MgO-Al_2O_3-SiO_2 system. *International Journal of Materials Research*. 2004;95(9): 793–805. https://doi.org/10.3139/146.017909

35. de Noirfontaine M. N., Tusseau-Nenez S., Girod-Labianca C., Pontikis V. CALPHAD formalism for Portland clinker: thermodynamic models and databases. *The Journal of Materials Science*. 2012;47: 1471–1479. https://doi.org/10.1007/s10853-011-5932-7

36. Shepherd E. S., Rankin G. A., Wright F. E. The binary systems of alumina with silica, lime and magnesia. *American Journal of Science*. 1909;(28): 293–333. Available at: https://zenodo.org/records/1633772

37. Klug F. J., Prochazka S. Alumina-silica phase diagram in the mullite region. *Journal of the American Ceramic Society*. 1987;70(10): 750–759. https://doi.org/10.1111/j.1151-2916.1987.tb04875.x

38. Aksay I. A., Pask J. A. Stable and metastable equilibria in the system SiO_2-Al_2O_3. *Journal of the American Ceramic Society*. 1975;58(10-14): 507–512. https://doi.org/10.1111/j.1151-2916.1975.tb18770.x

39. Shornikov S. I., Archakov I. Yu., Chemekova T. U. A mass spectrometry study of evaporation processes and phase equilibria in the Al_2O_3-SiO_2 system. *Russian Journal of Physical Chemistry A*. 2000;74(5): 684–688. Available at: https://elibrary.ru/item.asp?id=13347337

40. Eriksson G., Pelton A. D. Critical evaluation and optimization of the thermodynamic properties and phase diagrams of the CaO-Al_2O_3, Al_2O_3-SiO_2, and CaO-Al_2O_3-SiO_2 systems. *Metallurgical Transactions B*. 1993;24B: 807–816. https://doi.org/10.1007/BF02663141

41. Mao H., Selleby M., Sundman B. Phase equilibria and thermodynamics in the Al_2O_3-SiO_2 system - modeling of mullite and liquid. *Journal of the American Ceramic Society*. 2005;88(9): 2544–2551. https://doi.org/10.1111/j.1551-2916.2005.00440.x.

42. Yazhenskikh E., Hack K., Müller M. Critical thermodynamic evaluation of oxide systems relevant to fuel ashes and slags. Part 3: silica-alumina system. *CALPHAD*. 2008;32: 195–205. https://doi.org/10.1016/j.calphad.2007.05.004

43. Ban T., Hayashi S., Yasumori A., Okada K. Calculation of metastable immiscibility region in the Al_2O_3-SiO_2 system. *Journal of Materials Research*. 1996;11 (6): 1421-1427. https://doi.org/10.1557/jmr.1996.0178

44. Björkvall J., Stolyarova V. L. A mass spectrometric study of Al_2O_3-SiO_2 melts using a Knudsen cell. *Rapid Communications in Mass Spectrometry*. 2001;15(10): 836–842. https://doi.org/10.1002/rcm.251

45. Kwon S. Y., Jung I.-H. Thermodynamic assessment of the Al_2O_3-ZrO_2, CaO-Al_2O_3-ZrO_2, and Al_2O_3-SiO_2-ZrO_2 system. *Ceramics International*. 2022;48: 5413–5427. https://doi.org/10.1016/j.ceramint.2021.11.085

46. Lambotte G., Chartrand P. Thermodynamic evaluation and optimization of the Al_2O_3–SiO_2-AlF_3-SiF_4 reciprocal system using the modified quasichemical model. *Journal of the American Ceramic Society*. 2011;94: 4000–4008. https://doi.org/10.1111/j.1551-2916.2011.04656.x

47. Igami Y., Ohi S., Miyake A. Sillimanite-mullite transformation observed in synchrotron X-ray diffraction experiments. *Journal of the American Ceramic Society*. 2017;100: 4928–4937. https://doi.org/10.1111/jace.15020

48. Yarotskaya E. G., Fedorov P. P. Mullite and its isomorphic substitution. *Condensed Matter and Interphases*. 2018;20(4): 537–544. https://doi.org/10.17308/kcmf.2018.20/626

49. Saenko I., Ilatovskaia M., Savinykh G., Fabrichnaya O. Experimental investigation of phase relations and thermodynamic properties in the ZrO_2-TiO_2 system. *Journal of the American Ceramic Society*. 2018;101: 386–399. https://doi.org/10.1111/jace.15176

50. Troitzsch U., Ellis D. J. The ZrO_2-TiO_2 phase diagram. *Journal of Materials Research*. 2005;40(11): 4571–4577. https://doi.org/10.1007/s10853-005-1116-7

51. Ilatovskaia M., Savinykh G., Fabrichnaya O. Thermodynamic description of the Ti-Al-O system based on experimental data. *Journal of Phase Equilibria and Diffusion*. 2017;38 (3): 175–184. https://doi.org/10.1007/s11669-016-0509-4

52. Lang S., Fillmore C., Maxwell L. The system beryllia-alumina-titania: phase relations and general physical properties of three-component porcelains. *Journal of Research of the National Bureau of Standards*. 1952;48: 301–321. Available at: https://doi.org/10.6028/jres.048.038

53. Freudenberg B. *Etude de la reaction à l'état solide: Al_2O_3+TiO_2-Al_2TiO_5*. Tesis Doctoral. Ecôle Polytécnique, Lausanne. 1987. 262 p. https://doi.org/10.5075/epfl-thesis-709

54. de Arenas I. B. Reactive sintering of aluminum titanate. In: *Sintering of Ceramics-New Emerging Techniques*. Arunachalam Lakshmanan (ed.). InTech; 2012. p. 501–526. https://doi.org/10.5772/34366

55. Norberg S. T., Hoffmann S., Yoshimura M., Ishizawa N. $Al_6Ti_2O_{13}$, a new phase in the Al_2O_3-TiO_2 system. *Acta Crystallographica. Section C*. 2005;C61: i35-i38. https://doi.org/10.1107/s0108270105002532

56. Hoffmann S., Vasylechko L. O., Trots D. M., Yoshimura M. Thermal expansion of $Al_6Ti_2O_{13}$ between 20 K and 1173 K. *Zeitschrift für anorganische und allgemeine Chemie*. 2010;636: 2059–2059. https://doi.org/10.1002/zaac.201009020

57. Hoffmann S., Norberg S. T., Yoshimura M. Melt synthesis of Al_2TiO_5 containing composites and reinvestigation of the phase diagram Al_2O_3-TiO_2 by powder X-ray diffraction. *Journal of Electroceramics*. 2006;16: 327–330. https://doi.org/10.1007/s10832-006-9873-5

58. Berger M. H., Sayir A. Directional solidification of the Al_2O_3-Al_2TiO_5 system. *Journal of the European* Ceramic *Society*. 2008;28: 2411–2419. https://doi.org/10.1016/j.jeurceramsoc.2008.03.005

59. Jung I.-H., Eriksson G., Wu P., Pelton A. Thermodynamic modeling of the Al_2O_3-Ti_2O_3-TiO_2 system and its applications to the Fe-Al-Ti-O inclusion diagram. *ISIJ International*. 2009;49: 1290–1297. https://doi.org/10.2355/isijinternational.49.1290

60. Panda S. K., Jung I.-H. Coupled experimental study and thermodynamic modeling of the Al_2O_3-Ti_2O_3-TiO_2 system. *ISIJ International*. 2020:60: 31–41. https://doi.org/10.2355/isijinternational.ISIJINT-2019-006

61. Azimov S. A., Gulamova D. D. Mel'nik N. N., Sarkisova M. Kh., Suleimanov S. Kh., Tsapenko L. M. An investigation of aluminum titanate produced in the solar furnace*. *Izvestiya Akademii Nauk SSSR. Inorganic Matererials*. 1984;20(3): 469–471. (In Russ.)

62. Guljamova D. D., Sarkisova M. H. Interaction of aluminium and titanium oxides at high temperatures*. *Doklady Akademii Nauk SSSR. Inorganic Materials*. 1989;25(5): 789–794. (In Russ.)

63. Stolyarova V. L., Vorozhtcov V. A., Shemchuk D. V., Lopatin S. I., Bogdanov O. A. High temperature mass spectrometry study of the TiO_2-Al_2O_3 system. *Russian Journal of General Chemistry*. 2021;91(10): 1999–2007. https://doi.org/10.1134/S107036322110011X

64. Agamawi Y. M., White J. The system Al_2O_3-TiO_2-SiO_2. *Transactions of the British Ceramic Society*. 1952;51(5): 293–325.

65. Toropov N. A., Barzakovsky V. P., Lapshin V. V., Kurtseva N. N., Boikova A. I. *State diagrams of silicate systems. Reference book. Issue 3. Ternary silicate systems**. Leningrad, Nauka Publ.; 1972. 448 p. (In Russ.)

66. Galakhov F. Ya. The study of the alumina-rich area of aluminosilicate systems. Report 3. The TiO_2-Al_2O_3-SiO_2 system*. *Izvestiia Akademii Nauk SSSR. Seriia Khimicheskaia*. 1958;(5): 529–534. (In Russ.).

67. Fidancevska E., Vassilev V. Obtaining of powders by controlled hydrolysis and sintering of materials from the TiO_2-Al_2O_3-SiO_2 system. *Journal of Chemical Technology and Metallurgy*. 2010;45(4): 421–430. Available at: https://journal.uctm.edu/node/j2010-4/10_Venci_Vassilev_425-434.pdf

68. Ilatovskaia M., Bärtel F., Fabrichnaya O. Phase relations in the Al_2O_3-TiO_2-SiO_2 system. *Ceramics International*. 2020;46(18): Part B: 29402–29412. https://doi.org/10.1016/j.ceramint.2020.05.103

69. Budnikov P. P., Litvakovsky A. A. To study the Al_2O_3-SiO_2-ZrO_2 system*. *Bulletin of the Russian Academy of Sciences USSR*. 1956;106(2): 267. (In Russ.)

70. Greca M. C., Emiliano J. V., Segadães A. M. Revised phase equilibrium relationships in the system Al_2O_3-ZrO_2-SiO_2. *Journal of the European* Ceramic *Society*. 1992;9(4): 271–283. https://doi.org/10.1016/0955-2219(92)90062-I

71. Ferrari C. R., Rodrigues J. A. Microstructural features of alumina refractories with mullite-zirconia aggregates. *Boletín de la Sociedad Española de Cerámica y Vidrio*. 2003;42: 15–20. https://doi.org/10.3989/cyv.2003.v42.i1.651

72. Quereshi M. H., Brett N. H. Phase equilibria in ternary systems containing zirconia and silica. II. The system $A1_2O_3$-ZrO_2-SiO_2. *Transactions of the British Ceramic Society*. 1968;67(11): 569–579.

73. Pena P., De Aza S. The zircon thermal behavior: effect of impurities. *Journal of Materials Science*. 1984;19: 135–142. https://doi.org/10.1007/bf02403119

74. Pena P. Refractarios para zonas de contacto con el vidrio. *Boletín de la Sociedad Española de Cerámica y Vidrio*. 1989;28: 89–96. Available at: https://boletines.secv.es/upload/198928089.pdf

75. Sánchez Soto P. J., Pérez Rodríguez J. L. Características generales, propiedades, yacimientos y aplicaciones de pirofilita. II. Yacimientos, aplicaciones y utilización como materia prima cerámica. *Boletín de la Sociedad Española de Cerámica y Vidrio*. 1998;37: 359–368. https://doi.org/10.3989/cyv.1998.v37.i5.995

76. Vorob'eva V. P., Zelenaya A. E., Lutsyk V. I. Using a 3D computer model of the *T-x-y* diagram of the ZrO_2-SiO_2-Al_2O_3 system to resolve contradictions in the initial experimental data. *Russian Journal of Inorganic Chemystry*. 2021;66(6): 894–901. https://doi.org/10.1134/S003602362106022X

77. Ilatovskaia M., Savinykh G., Fabrichnaya O. Thermodynamic description of the ZrO_2-TiO_2-Al_2O_3 system based on experimental data. *Journal of the European* Ceramic *Society*. 2017;37(10): 3461–3469. https://doi.org/10.1016/j.jeurceramsoc.2017.03.064

78. Barzakovskii V. P., Lapin, V. V., Bojkova A. I., Kurtseva N. N. *State diagrams of silicate systems. The Handbook. Part 4: Ternary silicate systems**. Leningrad: Nauka Publ.; 1974. 514 p. (In Russ.).

79. http://www.crct.polymtl.ca/fact/phase_diagram.php?file=Al-Ti-Zr-O_Al2O3-TiO2-ZrO2_liquidus-projection.jpg&dir=FToxid

80. Coughanour L. W., Roth R. S., De Prosse V. A. Phase equilibrium relations in the system lime-titania and zirconia-titania. *Journal of Research of the National Bureau of Standards*. 1954;52(1): 37–42. Available at: https://nvlpubs.nist.gov/nistpubs/jres/52/jresv52n1p37_A1b.pdf

81. Shevchenko A. V., Lopato L. M., Meister I. M., Gorbunov O. S. ZrO_2-TiO_2 system*. *Russian Journal of Inorganic Chemystry*. 1980;25(9): 2496–2499. (In Russ.)

82. Pena P., De Aza S. El sistema ZrO_2-SiO_2-TiO_2. *Boletín de la Sociedad Española de Cerámica y Vidrio*. 1976;15(2): 93–95.

83. Belov G. V., Aristova N. M. Databases on the properties of materials and substances for nuclear power*. *Mathematical Models and Computer Simulations*. 2017;29(6): 135–142. Available at: http://mi.mathnet.ru/eng/mm/v29/i6/p135 (In Russ.)

84. Ohnuma I., Ishida K. Phase diagrams as tools for advanced materials design: applications to non-ferrous alloys. *Tecnologia em Metalurgia, Materiais e Mineração*. 2016;13(1): 46. http://dx.doi.org/10.4322/2176-1523.1085

85. Bakardjieva S., Barrachin M., Bechta S., … Wiss T. Quality improvements of thermodynamic data applied to corium interactions for severe accident modelling in SARNET2. *Annals of Nuclear Energy*. 2014;74: 110–124. https://doi.org/10.1016/j.anucene.2014.06.023

86. Kitagaki T., Yano K., Ogino H., Washiya T. Thermodynamic evaluation of the solidification phase of molten core-concrete under estimated Fukushima daiichi nuclear power plant accident conditions. *Journal of Nuclear Materials*. 2017;486: 206–215. https://doi.org/10.1016/j.jnucmat.2017.01.032

87. Bakardjieva S., Barrachin M., Bechta S., … Wiss T. Improvement of the european thermodynamic database NUCLEA. *Progress in Nuclear Energy*. 2010;52: 84–96. https://doi.org/10.1016/j.pnucene.2009.09.014

88. Kwon S. Y. *Thermodynamic optimization of ZrO_2-containing systems in the CaO-MgO-SiO_2-Al_2O_3-ZrO_2 system*. Dissertation. Department of mining and materials engineering. McGill University. Montreal, QC. 2015. 113 p. Available at: https://escholarship.mcgill.ca/concern/theses/dz010t00f

89. Lutsyk V. I., Vorob'eva V. P. Computer models of eutectic-type *T-x-y* diagrams with allotropy. Two inner liquidus fields of two low-temperature modifications of the

same component. *Journal of Thermal Analysis and Calorimetry*. 2010;101(1): 25–31. https://doi.org/10.1007/s10973-010-0855-0

90. Lutsyk V. I., Vorob'eva V. P. 3D Model of the *T*–*x*–*y* Diagram of the Bi-In-Sn System for designing microstructure of alloys. *Russian Journal of Inorganic Chemystry*. 2016;61(2): 188–207. https://doi.org/10.1134/S0036023616020121

91. Vorob'eva V. P., Zelenaya A. E., Lutsyk V. I., Sineva S. I., Starykh R. V., Novozhilova O. S. High-Temperature area of the Fe-Ni-Co-Cu diagram: experimental study and computer design. *Journal of Phase Equilibria and Diffusion*. 2021;42(2): 175–193. https://doi.org/10.1007/s11669-021-00863-3

92. Lutsyk I. V., Zelenaya A. E., Zyryanov A. M. Multicomponent systems simulation by the software of "Diagrams Designer". *Journal of International Scientific Publications: Materials, Methods and Technologies*. 2008;2(1): 176–184. Available at: https://www.scientific-publications.net/download/materials-methods-and-technologies-2008.pdf

93. Lutsyk V. I., Vorob'eva V. P. Three-dimensional model of phase diagram of Au-Bi-Sb system for clarification of thermodynamic calculations. *Russian Journal of Physical Chemistry*. 2015;89(10): 1715–1722. https://doi.org/10.1134/S0036024415100192

94. Lutsyk V. I., Vorob'eva V. P., Shodorova S. Ya. Verification of the *T*–*x*–*y* diagram of the Ag–Au–Bi system using a 3D computer model. *Russian Journal of Inorganic Chemystry*. 2016;61(7): 858–866. https://doi.org/10.1134/S0036023616070123

95. Nasrulin E. R., Lutsyk V. I., Vorobyova V. P. *Visualization of crystallization paths and calculation of material balance in ternary phase diagrams**. Copyright certificate of RF No. 50200601390; ESPD.03524577.01520-01; No. 6632; application 06/29/2006; Publ. 08.08.2006 (In Russ.)

96. Lutsyk V. I., Vorob'eva V. P., Zelenaya A. E. 3D reference book on the oxide systems space diagrams as a tool for data mining. *Solid State Phenomena*. 2015;230: 51–54. https://doi.org/10.4028/www.scientific.net/ssp.230.51

97. Vorob'eva V. P., Zelenaya A. E., Lutsyk V. I. Analysis of the geometric features of *T*-*x*-*y* diagrams with melt immiscibility for silicate systems. *Journal of Physics: Conference Series*. 2021;1791(1): 012121. https://doi.org/10.1088/1742-6596/1791/1/012121

98. Vorob'eva V. P., Zelenaya A. E., Lutsyk V. I., Lamueva M. V. A 3D computer model of the CaO-MgO-Al_2O_3 *T*-*x*-*y* diagram at temperatures above 1300 °C. *Condensed Matter and Interphases*. 2021;23(3): 380–386. https://doi.org/10.17308/kcmf.2021.23/3529

99. Lutsyk V. I., Zelenaya A. E., Savinov V. V. Phase trajectories in CaO-Al_2O_3-SiO_2 melts. *Crystallography Reports*. 2012;57(7): 943–947. https://doi.org/10.1134/s1063774512070176

100. Lutsyk V., Zelenaya A. Crystallization paths in SiO_2-Al_2O_3-CaO system as a genotype of silicate materials. *IOP Conference Series: Materials Science and Engineering*. 2013;47: 012047. https://doi.org/10.1088/1757-899x/47/1/012047

101. Lutsyk I. V., Zelenaya A. E., Nasrulin E. R., Zyryanov A. M. The NaCl-$CaCl_2$-$MgCl_2$ system: analysis of zero-, one- and two-dimensional concentration fields. *Melts*. 2016;(3): 216–225. Available at: https://www.elibrary.ru/item.asp?id=27184380 (In Russ.)

102. Lutsyk V. I., Zelenaya A. E. *T*-*x*-*y* diagram of the MgO-SiO_2-Al_2O_3 system: microstructure design. *Russian Journal of Inorganic Chemistry*. 2018;63(8): 1087–1091. https://doi.org/10.1134/S0036023618080132

103. Connell R. G. A tutorial on flow diagrams: a tool for developing the structure of multicomponent phase diagrams. *Journal of Phase Equilibria and Diffusion*. 1994;15(1): 6–19. https://doi.org/10.1007/BF02667677

104. Vorozhtcov V. A., Yurchenko D. A., Almjashev V. I., Stolyarova V. L. Phase equilibria in the Al_2O_3-SiO_2-ZrO_2 system: calculation and experiment. *Glass Physics and Chemistry*. 2021;47: 417–426. https://doi.org/10.1134/S1087659621050175

105. Vorob'eva V. P., Zelenaya A. E., Lutsyk V. I., Vorozhtcov V. A., Almjashev V. I., Stolyarova V. L. State diagram of the ZrO_2-SiO_2-Al_2O_3 system with visualization by 3D computer model and calculation using the NUCLEA database. *Doklady Physical Chemistry*. 2023;511(1): 107–116. https://doi.org/10.1134/S0012501623600079

106. Vorob'eva V. P., Zelenaya A. E., Lutsyk V. I., Vorozhtcov V. A., Almjashev V. I., Sokolova T. V., Stolyarova V. L. Modeling of the ZrO_2-SiO_2-Al_2O_3 phase diagram using simulation by the 3D computer model and the NUCLEA database. *Materials Science and Engineering B*. 2023;297: 116790. https://doi.org/10.1016/j.mseb.2023.116790

107. Lutsyk V., Zelenaya A., Zyryanov A., Nasrulin E. Computer models of phase diagrams for ceramic systems. TiO_2-SiO_2-Al_2O_3 and ZrO_2-SiO_2-Al_2O_3. *Epitoanyag - Journal of Silicate Based and Composite Materials*. 2016;68(2): 52–55. https://doi.org/10.14382/epitoanyag-jsbcm.2016.9

108. Vorob'eva V. P., Zelenaya A. E., Lutsyk V. I., Almjashev V. I., Vorozhtcov V. A., Stolyarova V. L. Prediction of the liquidus of the quaternary system of titanium, aluminim, silicon, and zirconium oxides. *Glass Physics and Chemistry*. 2021;47(6): 616–621. https://doi.org/10.1134/S1087659621060328

* *Translated by author of the article*

Information about the authors

Vasily I. Lutsyk, Dr. Sci. (Chem.), Head of Sector of Computer Materials Design, Institute of Physical Materials Science of Siberian Branch of Russian Academy of Sciences (Ulan-Ude, Russian Federation).

https://orcid.org/0000-0002-6175-0329

vluts@ipms.bscnet.ru

Anna E. Zelenaya, Cand. Sci. (Phys.-math.), Senior Researcher of Sector of Computer Materials Design, Institute of Physical Materials Science of Siberian Branch of Russian Academy of Sciences (Ulan-Ude, Russian Federation).

https://orcid.org/0000-0001-5232-8567

zel_ann@mail.ru

Vera V. Vorob'eva, Dr. Sci. (Phys.-math.), Leading Researcher of Sector of Computer Materials Design, Institute of Physical Materials Science of Siberian Branch of Russian Academy of Sciences (Ulan-Ude, Russian Federation).

https://orcid.org/0000-0002-2714-3808

vvorobjeva@mail.ru

Received 28.06.2024; approved after reviewing 08.07.2024; accepted for publication 16.09.2024; published online 25.12.2024.

Translated by Irina Charychanskaya